

A New Scheme of Nonlinear Energy Transfer among Wind Waves: RIAM Method —Algorithm and Performance—

KOSEI KOMATSU^{1*} and AKIRA MASUDA²

¹*Department of Earth System Science & Technology, Graduate School of Engineering Sciences,
Kyushu University, Kasuga 816, Japan*

²*Research Institute for Applied Mechanics, Kyushu University, Kasuga 816, Japan*

(Received 16 October 1995; in revised form 4 January 1996; accepted 25 January 1996)

A numerical scheme for calculating the nonlinear energy transfer among wind waves (RIAM method) was developed on the basis of the rigorous method of Masuda. Then the performance of the RIAM method was examined by applying it to various forms of wind-wave spectra and different situations of wind-wave evolution, in comparison mainly with the WAM method. The computational time of the Masuda method was reduced by a factor of 300 by the RIAM method, which is still 2000 times slower than the WAM method simply because the RIAM method processes thousands of resonance configurations whereas the WAM method does only one. The RIAM method proves to give accurate results even for spectra of narrow band widths or bimodal spectra, whereas the WAM method often calculates an unrealistic magnitude and pattern of nonlinear energy transfer functions. In the duration-limited evolution of wind-wave spectra, the RIAM method yields a unimodal directional distribution on the low-frequency side of the spectral peak, whereas the WAM method produces a spurious bimodal one there. At higher frequencies, however, both methods give a bimodal directional distribution with two oblique maxima. The RIAM method enhances the growth of the total energy and peak period of wind waves in comparison with the WAM method. Nevertheless, Toba's constant of his 3/2-power law approaches almost the same standard value of 0.06 in both methods. For spectra of a narrow band width or for those perturbed by a small hump or depression, the RIAM method tends to recover the monotonic smoother form of spectrum whereas the WAM method often yields unrealistic humps or depressions.

1. Introduction

Wave prediction today is based on the equation of energy balance for each spectral component. For deep water the evolution of the spectral component is governed by

$$\frac{\partial F}{\partial t} + C_g \cdot \nabla F = I + T + D \quad (1)$$

in the absence of surface currents, where $F = F(\mathbf{k}; \mathbf{x}, t)$ denotes the two-dimensional spectrum with

*Present affiliation: Research Institute for Applied Mechanics, Kyushu University, Kasuga 816, Japan.

respect to the wavenumber k at the horizontal position x and time t . The terms on the left-hand side indicate the local change and the energy radiation at the group velocity C_g , respectively, while those on the right-hand side represent the source functions: I is the energy input due to wind, T the nonlinear energy transfer function due to resonant wave-wave interaction, and D the energy dissipation mainly due to wave breaking. Each of the source functions therefore must be estimated precisely in order to predict the evolution of wave spectra accurately.

Among the three source terms, the nonlinear energy transfer due to four-wave resonance has been considered one of the most important factors that control the evolution of wave spectra: down shift of the spectral peak frequency, self-stabilization of the spectral form, and frequency-dependent redistribution of angular distribution functions. Although the formulation of this mechanism for continuous spectra was accomplished by Hasselmann as early as 1962 (Hasselmann, 1962, 1963), the precise evaluation of nonlinear energy transfer functions requires considerable efforts since it is expressed as a triple integration with singular points. Sell and Hasselmann (1973) first presented a systematic numerical computation of the nonlinear energy transfer function for the Pierson-Moskowitz spectrum (abbreviated as the PM spectrum) and the JONSWAP spectrum. Their results, however, somewhat lack in numerical stability and showed that even the spectral peak can gain energy through nonlinear energy transfer. This conclusion appeared unacceptable intuitively at those days, because nonlinear energy transfer was generally supposed to redistribute energy in a smoothing way (Phillips, 1977). This is why many works followed Sell and Hasselmann to elucidate what the *true* energy transfer should be like (Longuet-Higgins, 1976; Fox, 1976; Webb, 1978; Dungey and Hui, 1979). The controversy was decisively resolved by Masuda (1980, 1986), who showed how the contradiction arose on the basis of a stable and rigorous algorithm developed by himself. Applying his algorithm to different forms of wind-wave spectra, he also pointed out that the nonlinear transfer function *sensitively* depends on the spectral forms both in magnitude and in pattern. Successive efforts based on other rigorous schemes have still been continued to reveal various properties of nonlinear energy transfer (for example, Hasselmann and Hasselmann, 1985; Young *et al.*, 1987; Resio and Perrie, 1991).

Nevertheless, the exact computation of nonlinear transfer functions consumes still too much time to be incorporated in operational models for wave forecast. First-generation models therefore totally discarded the nonlinear energy transfer function except implicitly through dissipation terms. Also second-generation models have abandoned the computation of nonlinear energy transfer functions by restricting the prediction only to several parameters that characterize wind-wave spectra; detailed spectra are determined according to some empirical form of wave-spectra in generation areas. That is, second-generation models take the nonlinear transfer function into account in an implicit way through empirical forms of spectra, which should be controlled by nonlinear energy transfer. It became clear, however, that no model participating in the SWAMP Group (1985) intercomparison study could properly simulate the complex wind-seas resulting from a sudden change of wind. This inadaptability of the models of the second generation was ascribed to their insufficient degree of freedom, which is an unavoidable consequence of the parametric representation of wave spectra.

The deficiency was overcome soon by the development of the wave-forecasting model of the third generation, in which nonlinear energy transfer functions are computed explicitly. The WAM model (WAMDI Group, 1988) is a representative one that belongs to this generation. It calculates nonlinear transfer functions explicitly according to the discrete interaction approximation (Hasselmann *et al.*, 1985). Young *et al.* (1987) showed that, even for abruptly changing wind fields, the WAM model fairly closely reproduced the wave evolution evaluated with the

EXACT-NL model based on the exact calculation of nonlinear energy transfer (Hasselmann and Hasselmann, 1985). It must be noted, however, that the discrete interaction approximation (or the WAM method henceforth), is a crudest way for computing nonlinear energy transfer functions. Strikingly enough, the WAM method substitutes a *single* configuration of resonant four waves for an *infinite* numbers of configurations. Accordingly, the WAM method is considered to have a rather limited validity, as will be shown later. In this sense, the WAM method should be replaced by a better one in order to improve the performance of wave models and in order to gain a better physical understanding of the evolution of wind-wave spectra. It is indispensable for the desired algorithm to compute nonlinear energy transfer functions with sufficient accuracy for any kind of spectral forms. The rigorous method, which may be precise but consumes tremendous computational time, is not suitable for operational wave-forecasting models of the next generation.

Thus, it is necessary to develop a method equipped with both practically sufficient accuracy and efficiency suitable for practical wave forecasting models with a general adaptability. In order to present a candidate for or a starting one toward such a method, we begin with the rigorous method of Masuda (1980), which has a high precision through its analytical processing of singular points. Then, making full use of the symmetry of resonant interaction (cf. Hasselmann and Hasselmann, 1981) and truncating less substantial configurations of resonance, we develop an algorithm that achieves shorter computational time without serious loss of accuracy. The primary purpose of this paper is therefore to present some details of this new method and to compare its performance with that of other available schemes, in particular, of the WAM method, which is adopted in a most popular operational model. The performance is examined in the evolution of wind-wave spectra as well. The dynamics, however, will be argued in another paper, as to how wind-wave spectra evolve driven by three source terms parameterized in the wave model or what kind of equilibrium is realized in saturated spectra.

The next section describes the algorithm of the new method, which is to be called as the RIAM* method henceforth. We examine the basic properties of the RIAM method such as its computational time, accuracy, and parameter sensitivity. Then the RIAM method is applied to several cases of temporal evolution of wave spectra to be compared with those due to the WAM method. Finally, a summary and discussions are given in Section 4.

2. Algorithm and Basic Properties of the RIAM Method

The nonlinear energy transfer function $T(\mathbf{k}_4)$ at the wave number \mathbf{k}_4 is expressed by the Boltzmann integral (Hasselmann, 1962, 1963):

$$T(\mathbf{k}_4) = \omega_4 \int \cdots \int d\mathbf{k}_1 d\mathbf{k}_2 d\mathbf{k}_3 G(\mathbf{k}_1, \mathbf{k}_2, \mathbf{k}_3, \mathbf{k}_4) \delta(\mathbf{k}_1 + \mathbf{k}_2 - \mathbf{k}_3 - \mathbf{k}_4) \times \delta(\omega_1 + \omega_2 - \omega_3 - \omega_4) \{n_1 n_2 (n_3 + n_4) - n_3 n_4 (n_1 + n_2)\}, \quad (2)$$

where $n_i = n(\mathbf{k}_i) = F(\mathbf{k}_i)/\omega_i$ ($i = 1, 2, 3,$ and 4) denotes the action density for the wavenumber \mathbf{k}_i , $\omega_i = |\mathbf{g}\mathbf{k}_i|^{1/2}$ the corresponding angular frequency with \mathbf{g} the acceleration due to gravity, and G the coupling coefficient (Hasselmann, 1963). The delta function δ means that nonlinear interaction occurs among wave components which satisfy the four-wave resonance conditions:

*Research Institute for Applied Mechanics.

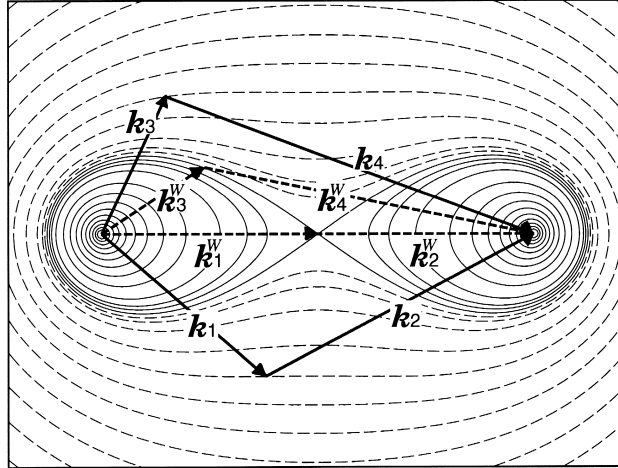


Fig. 1. *Figure of eight* representing the conditions for the four-wave resonance: contours of γ defined in Masuda (1980). This figure shows that a pair of wavenumbers k_3 and k_4 resonate with another pair of k_1 and k_2 , such that $k_3 + k_4 = k_1 + k_2$, only when they lie on the same contour of γ . Here and henceforth solid and dashed lines indicate positive and negative contours, respectively. The contour values are $\pm(0.0, 0.005, 0.01, 0.02, 0.04, 0.06, 0.08, 0.10, 0.12, 0.14, 0.16, 0.18)$. The RIAM method deals with about 2000 configurations among an infinite ones, while the WAM method uses only one configuration, which is designated by the thick dashed arrows with a superfix (W).

$$k_1 + k_2 = k_3 + k_4, \quad (3)$$

$$\omega_1 + \omega_2 = \omega_3 + \omega_4. \quad (4)$$

There are infinite number of possible configurations of resonant four wavenumbers, as shown by the *figure of eight* in Fig. 1 (Longuet-Higgins, 1962).

In order to develop a scheme of wider applicability than that of the WAM method, we follow the algorithm of Masuda (1980), which is excellent in accuracy and numerical stability or smoothness, but it consumes too much computational time for practical use. In this paper, we therefore improve his algorithm to develop a new method as efficient as possible for future models of wave prediction.

The highly technical portion of the algorithm was described in our preliminary report (Masuda, 1980; Komatsu *et al.*, 1993), so that we only give a brief sketch of the scheme. The most significant revision to that report is that the outermost *loop* of computation is now the *configuration*, instead of the frequency ω_4 of the largest wavenumber among resonant four component waves. It is to be noted that the actual algorithm is described in terms of the angular frequency ω and the propagation direction θ rather than the wavenumber k .

2.1 Algorithm

In order to save computational time, we take advantage of the symmetry of the integrand as in Hasselmann and Hasselmann (1981) or Resio and Perrie (1991). In here, two kinds of symmetry are discriminated from each other. The first kind is based on the well-known nature

of the nonlinear resonant interaction among gravity waves expressed by integral formula (2). Consider a particular combination of four resonant waves with wavenumber vectors \mathbf{k}_i ($i = 1, 2, 3,$ and 4). As explained in Hasselmann and Hasselmann (1981), $\delta n(\mathbf{k}_i) d\mathbf{k}_i / \delta t$ ($i = 1, 2, 3,$ and 4) are the same in magnitude, where $\delta n(\mathbf{k}) / \delta t$ indicates the action transfer that is due to this particular resonance combination. In addition, the lowest and the highest frequencies of the resonant four waves make the pair of the outer frequencies, while the other frequencies make the inner frequencies. The resonance deprives energy of the inner pair to supply it to the outer pair, or vice versa (Masuda, 1986). Accordingly, if we calculate $\delta n(\mathbf{k}) / \delta t$ for one component of the resonant four waves, then we immediately know $\delta n(\mathbf{k}) / \delta t$ for the other three components. The action transfers above for the four waves are converted into the corresponding nonlinear energy transfers due to that specific combination of resonance δT^{LO} , δT^{LI} , δT^{HI} , and δT^{HO} , where the suffixes on the shoulder *LO*, *LI*, *HI*, and *HO* denote the components of the lower frequency of the outer pair (LO component), the lower frequency of the inner pair (LI component), the higher frequency of the inner pair (HI component), and the higher frequency of the outer pair (HO component), respectively. This property reduces computational time by a factor of 4.

The second kind of symmetry is associated with the geometrical similarity of resonance configurations. First of all the mirror image of a resonance combination is also another one with the same interaction coefficient. Secondly, a rotation of a resonance combination gives another one with the same interaction coefficient. Thirdly, a scale transform of wavenumbers preserves the resonance condition. Though this last property is valid only for deep water waves, it allows us to estimate the interaction coefficient simply by multiplication of a certain power of the scale ratio (Masuda, 1980).

In order to make use of the symmetries mentioned above, the (ω, θ) space is divided into bins of nonuniform finite areas (Hasselmann and Hasselmann, 1981; Resio and Perrie, 1991). The central frequency ω_k of each bin is distributed on a logarithmic scale from the minimum frequency ω_{\min} to the maximum ω_{\max} at a constant ratio

$$R_\omega \equiv 1 + \Delta(\log \omega) \quad (5)$$

as

$$\omega_{k+1} = R_\omega \cdot \omega_k, \quad (6)$$

while the central direction θ_m of the bin is distributed as

$$\theta_{m+1} = \theta_m + \Delta\theta \quad (7)$$

with the directional increment $\Delta\theta$ kept constant. By virtue of this distribution of bins, the second kind of symmetry is expressed as follows. If a combination of certain four bins satisfies the resonance condition, so do any combinations of four bins that are obtained from the original combination through the (1) mirror transform, (2) rotational transform, and (3) scale transform. All the resonance *combinations* with the same geometry within the transforms above are said to have the same *configuration* of resonance.

Finally, the procedure is written schematically as

$$T = \sum_{cnf} \sum_{scl} \sum_{rot} (\delta T^{LO} + \delta T^{LI} + \delta T^{HI} + \delta T^{HO}), \quad (8)$$

where parameters cnf , scl , and rot symbolically denote the configuration, scale, and rotation (plus mirror image), respectively. The summation over the LO, LI, HI, and HO components represent the symmetry of the first kind, while the summation over cnf , scl , and rot correspond to the symmetry of the second kind. In order to limit the number of the resonance combinations, we discard the resonance configurations for which the ratio of the higher and lower frequencies of the outer pair ω^{HO}/ω^{LO} exceeds a prescribed value of C_r defined later.

In the RIAM method, the energy transfer is calculated for each bin. When we fix cnf , scl , rot , and a bin corresponding to the HO component (HO bin), the locations of the other three resonant bins relative to the HO bin in the frequency-direction space are determined according to the cnf parameter. The rate of energy the HO bin receives through the resonance among the four bins of assigned areas is calculated as

$$dT^{HO} = G_1(cnf) \cdot G_2(scl) \left(n^{LI} n^{HI} (n^{LO} + n^{HO}) - n^{LO} n^{HO} (n^{LI} + n^{HI}) \right), \quad (9)$$

where n^{LI} denotes the action density for the LI bin, and so on. In here, the two factors G_1 and G_2 describe the strength of the resonant interaction among the four bins. The kernel G_1 is determined easily by means of the Masuda method, because the resonance configuration is fixed and the properties of the bins are known; if the configuration is a singular one, it is to be dealt with analytically (Masuda, 1980; Komatsu *et al.*, 1993). On the other hand, G_2 is a simple power of the frequency of the HO bin (Masuda, 1980). Note that the resonance configuration, G_1 , and G_2 are independent of the details of the spectrum. Thus, we can determine beforehand the resonance configurations of the bins and the associated kernel G_1 , which is rather complicated.

Once δT^{HO} is obtained, it is easy to calculate the energy of the other resonant bins receive by virtue of the symmetry of the first kind. Then, the total nonlinear energy transfer is expressed as in (8).

2.2 Notations for wave spectra and nonlinear energy transfer functions

The two-dimensional wind-wave spectrum $F(\omega, \theta)$ is rewritten as

$$F(\omega, \theta) = F_1(\omega) S(\omega, \theta), \quad (10)$$

where $F_1(\omega)$ denotes the one-dimensional (frequency) spectrum and $S(\omega, \theta)$ the directional distribution (angular distribution function) satisfying

$$\int_{-\pi}^{+\pi} S(\omega, \theta) d\theta = 1. \quad (11)$$

Most of the frequency spectra F_1 examined here are those of the JONSWAP type (Hasselmann *et al.*, 1973)

$$F_1(\omega) = F_j(\omega; \gamma) \equiv \alpha g^2 \omega^{-5} \exp \left[-\frac{5}{4} \left(\frac{\omega}{\omega_p} \right)^{-4} \right] \gamma \exp \left[-\frac{(\omega - \omega_p)^2}{2\sigma^2 \omega_p^2} \right] \quad (12)$$

with the spectral peak frequency ω_p , Phillips' parameter α , peak-enhancement parameter γ , and

$$\sigma = \begin{cases} 0.07, & \omega \leq \omega_p \\ 0.09, & \omega > \omega_p. \end{cases} \quad (13)$$

The PM spectrum and the standard JONSWAP spectrum are recovered by putting $\gamma = 1$ and $\gamma = 3.3$, respectively.

On the other hand a most familiar expression for the directional distribution is

$$S(\omega, \theta) = \begin{cases} \hat{S}(s) \cos^s(\theta - \bar{\theta}), & 0 \leq |\theta - \bar{\theta}| \leq \pi/2 \\ 0, & \text{otherwise} \end{cases} \quad (14)$$

where $\hat{S}(s)$ is the normalization factor and $\bar{\theta}$ denotes the average wave direction, which will be put at zero unless stated otherwise. The parameter s , an index of directional concentration, may or may not depend on the frequency. A frequency-dependent form that has been supposed to represent the observed wind sea well is due to Mitsuyasu *et al.* (1975) and Hasselmann *et al.* (1980):

$$S(\omega, \theta) = \hat{S}(s) \cos^{2s} \left(\frac{\theta - \bar{\theta}}{2} \right), \quad (15)$$

where

$$s = 10^{0.99} \left(\frac{\omega}{\omega_p} \right)^b, \quad (16)$$

$$b = \begin{cases} 4.06, & \omega < \omega_p \\ -2.34, & \omega \geq \omega_p. \end{cases} \quad (17)$$

A somewhat novel form of directional spreading was proposed by Donelan *et al.* (1985):

$$S(\omega, \theta) = \frac{\beta}{2} \operatorname{sech}^2 \beta (\theta - \bar{\theta}), \quad (18)$$

where

$$\beta = \begin{cases} 2.61(\omega / \omega_p)^{+1.3}, & 0.56 \leq \omega / \omega_p < 0.95 \\ 2.28(\omega / \omega_p)^{-1.3}, & 0.95 \leq \omega / \omega_p < 1.6 \\ 1.24, & \text{otherwise.} \end{cases} \quad (19)$$

Instead of the two-dimensional $T(\omega, \theta)$, we often use

$$T_1(\omega) = \int_{-\pi}^{+\pi} T(\omega, \theta) d\theta \quad (20)$$

as its concise representation. Also, we usually nondimensionalize the frequency ω and frequency spectrum $F_1(\omega)$ so that both the peak frequency and the peak spectral density equal to unity. The dimensional T is obtained by multiplying its nondimensional value by the dimensional value of $F_1^3(\omega_p)\omega_p^{11}g^{-4}$.

2.3 Computational efficiency and accuracy of the RIAM method

Applied to typical spectra, the RIAM algorithm turned out to compute the nonlinear energy transfer function about 300 times faster than the original Masuda method, when we put almost the same conditions for computation mentioned below. The RIAM method, however, still requires 2000 times longer computational time than the WAM method. This is simply because the RIAM method processes thousands of resonance configurations whereas the WAM method

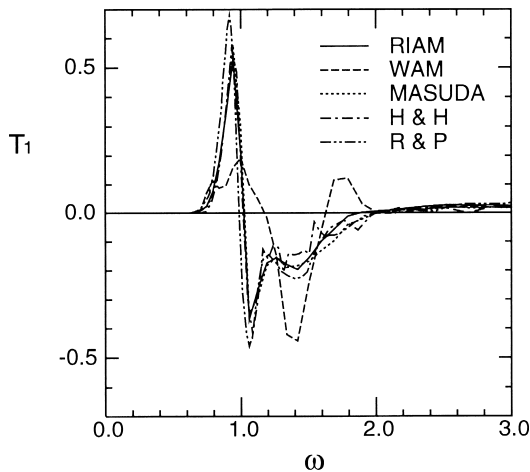


Fig. 2. Comparison of the one-dimensional transfer functions T_1 obtained by the RIAM method, the WAM method, Masuda (1980), Hasselmann and Hasselmann (H & H 1981), and Resio and Perrie (R & P 1991), where the wave spectrum examined is the standard JONSWAP frequency spectrum with $\cos^2\theta$ directional spreading. The transfer function is made nondimensional by the peak angular frequency ω_p and the peak spectral density $F_1(\omega_p)$. The parameters for the RIAM method are $R_\omega = 1.06$, $\Delta\theta = 10^\circ$, and $C_r = 3$, while those for the Masuda method are $R_\omega = 1.06$, $\Delta\theta = 10^\circ$, and $C_r = 7$.

deals with only one configuration. See Komatsu *et al.* (1993) for further details. For the present power of computers therefore the RIAM method is not fast enough for an operational model. With respect to accuracy, however, the RIAM method turns out to have much better performance in comparison with the prevalent WAM method, which often gives an unrealistic magnitude and pattern of nonlinear energy transfer functions, as will be shown later. The greatest advantage of the RIAM method is that it can be used as an efficient and almost rigorous method. It must be

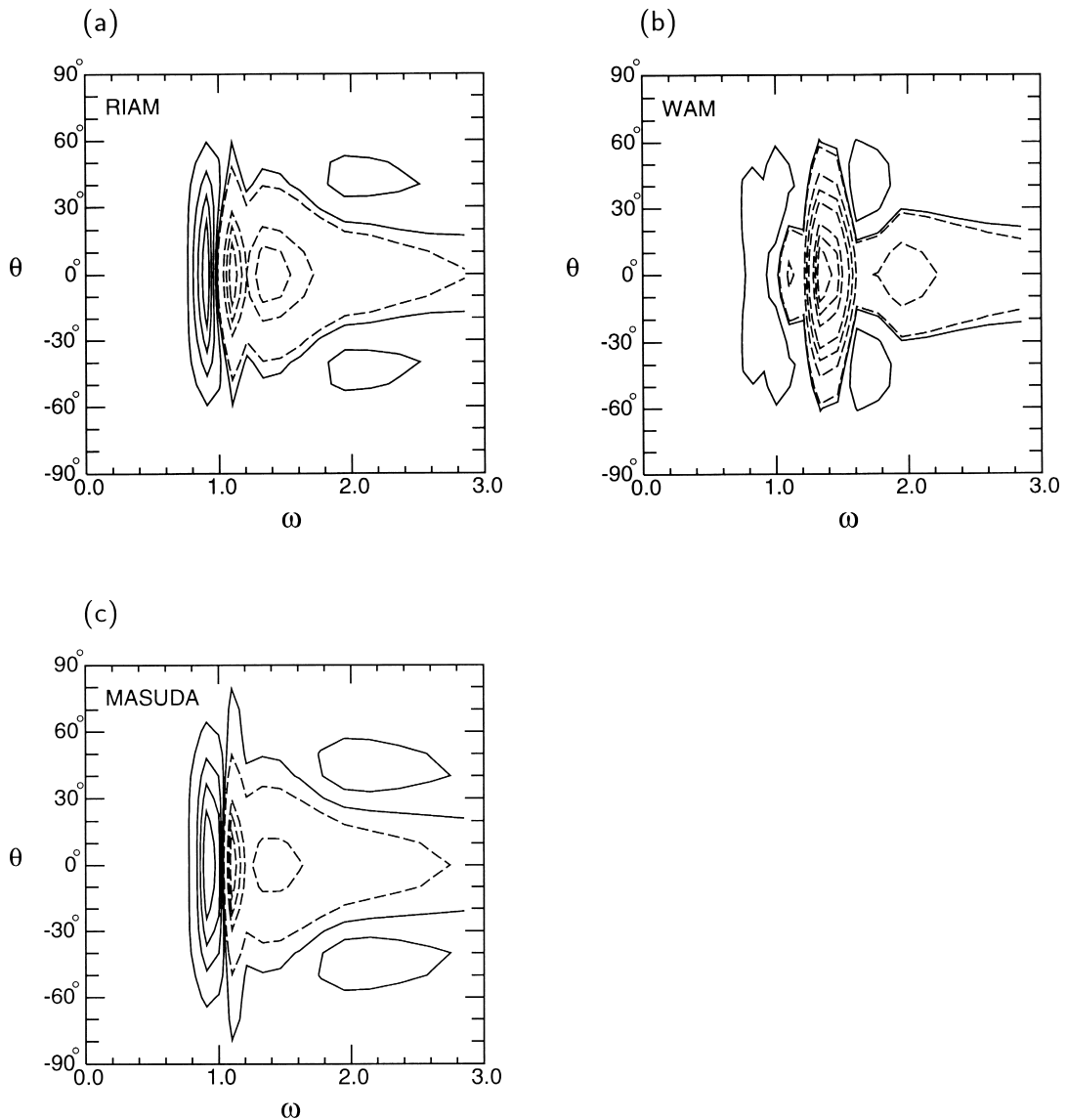


Fig. 3. Comparison of the two-dimensional energy transfer $T(\omega, \theta)$ obtained by (a) the RIAM method, (b) the WAM method, and (c) the Masuda method, where the model parameters and the wave spectrum examined are the same as in Fig. 2. The contour intervals are (a) 7.62×10^{-2} , (b) 3.74×10^{-2} , and (c) 7.25×10^{-2} . Note that the contour interval in (b) due to the WAM method is nearly half of the others.

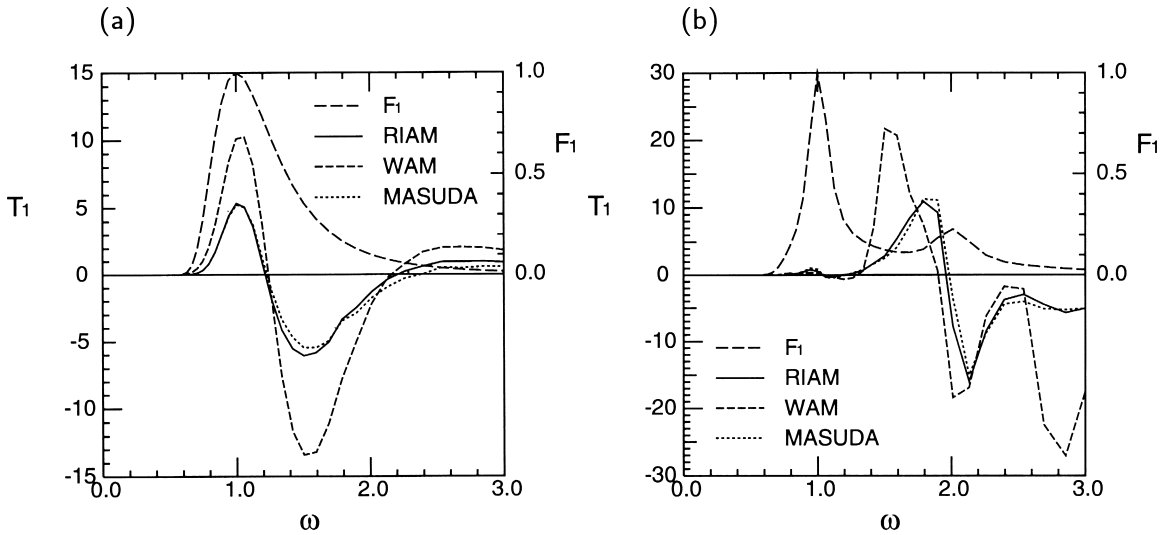


Fig. 4. Comparison of the one-dimensional energy transfer T_1 obtained by the RIAM method and the WAM method, where the wave spectrum examined is (a) the PM spectrum with $\cos^{10}\theta$ directional spreading $F(\omega, \theta) = F_J(\omega; 1) \hat{S}(10) \cos^{10}\theta$, and (b) a double-peaked spectrum with $\cos^2\theta$ directional spreading $F(\omega, \theta) = (F_J(\omega; 3.3) + 0.2 \times F_J(\omega/2; 3.3)) \hat{S}(2) \cos^2\theta$ (see the text for the other notations). The accuracy is examined by referring to the result through the rigorous algorithm of the Masuda method. The model parameters are the same as in Fig. 2.

noted that, throughout the paper, the *WAM method* simply means the method based on the same discrete interaction approximation that was employed in the WAM model, so that the remainder of the algorithm is the same as in the RIAM method. For better comparison, we tried to keep the resolution at the similar level to that for the standard RIAM method: $R_\omega = 1.1$, $\Delta\theta = 10^\circ$, and $C_r = 3$; the dependence of the performance of the RIAM method on these parameters will be discussed later.

We chose rather fine resolution of $R_\omega = 1.06$ in this subsection, where the accuracy of the RIAM method is compared with that of the WAM method or other rigorous algorithms. This is because Hasselmann and Hasselmann and Resio and Perrie used even finer resolution of $R_\omega < 1.02$, though we set $R_\omega = 1.06$ for the Masuda method; later the result with the RIAM method of $R_\omega = 1.06$ will be shown in fairly good agreement with that obtained at the standard resolution $R_\omega = 1.1$ (Fig. 5).

For the standard JONSWAP spectrum ($\gamma = 3.3$) with $\cos^2\theta$ directional spreading, Fig. 2 compares T_1 obtained by the present RIAM method with those by the WAM method or by previous rigorous algorithms: Masuda (1980), Hasselmann and Hasselmann (1981), and Resio and Perrie (1991). Among the rigorous methods we find that the Masuda or the Resio and Perrie method provides smoother T_1 than that by Hasselmann and Hasselmann, probably due to the adequate processing of singular points in the former two. The Masuda method gives almost the same values as the Hasselmann and Hasselmann method, while a slightly larger estimate is found in the Resio and Perrie method.

Figure 3 compares the two-dimensional distributions $T(\omega, \theta)$ calculated by the RIAM

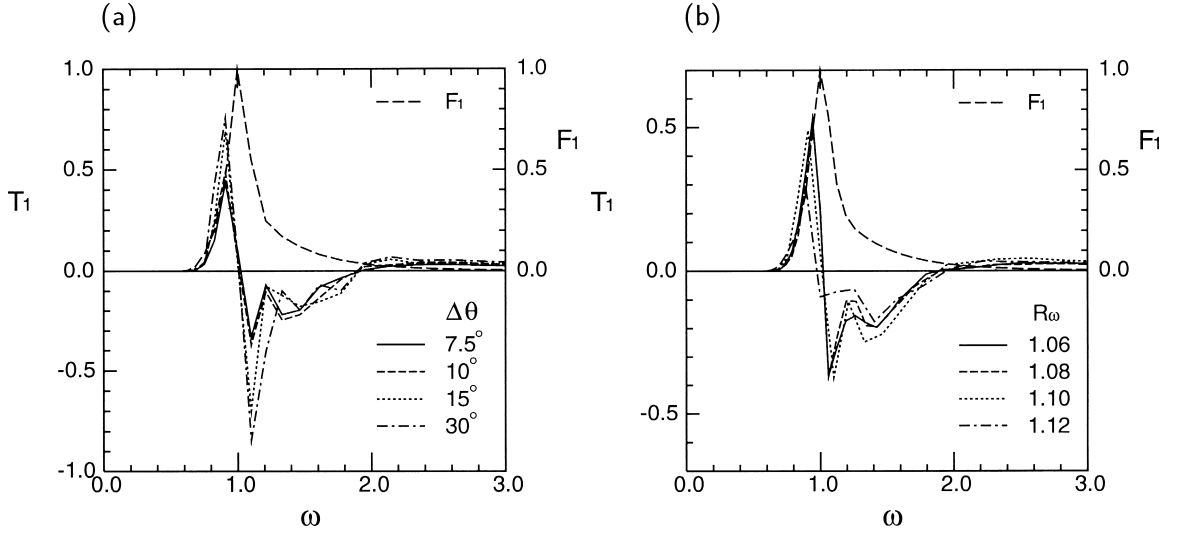


Fig. 5. Sensitivity of $T_1(\omega)$ computed with the RIAM method to the grid resolution for the same JONSWAP spectrum as in Fig. 2: (a) the angular mesh size $\Delta\theta$ is varied as 30° , 15° , 10° , and 7.5° , with R_ω fixed at 1.1 and (b) the frequency grid size is decreased as $R_\omega = 1.12$, 1.10, 1.08, and 1.06 with $\Delta\theta$ fixed at 10° , where $C_r = 3$ always.

method, the WAM method, and the Masuda method, for the same nonlinear energy transfer functions as in Fig. 2. Obviously, the RIAM method well reproduces T obtained with the Masuda method, whereas the WAM method completely differs from the others as well as in Fig. 2. In particular, we note that the WAM method yields a bimodal directional distribution with peaks around $\pm 30^\circ$ near $\omega \approx 0.8$. This curious bimodality is interpreted as a consequence of the preferred outflow of the energy to waves propagating at angles around $\pm 30^\circ$ in the discrete interaction approximation adopted in the WAM model.

These results show that the RIAM method preserves the same degree of accuracy and smoothness as the Masuda method. The WAM method, on the other hand, gives a completely different T both in magnitude and in pattern. It is to be noted that the spectrum examined was the standard JONSWAP spectrum, which is quite common and typical. Apparently, the WAM method lacks reliable accuracy for more precise forecast, even though its high speed has been highly evaluated.

The superiority of the RIAM method to the WAM method in accuracy is demonstrated more clearly for spectra with a narrow directional distribution or double-peaked spectra in the frequency domain, where accuracy is judged by the rigorous method of Masuda. Figure 4 shows T_1 for the PM spectrum with $\cos^{10}\theta$ directional spreading

$$F(\omega, \theta) = F_j(\omega; 1) \hat{S}(10) \cos^{10} \theta \quad (21)$$

and for a double-peaked spectrum with $\cos^2\theta$ directional spreading

$$F(\omega, \theta) = (F_j(\omega; 3.3) + 0.2 \times F_j(\omega / 2; 3.3)) \hat{S}(2) \cos^2 \theta. \quad (22)$$

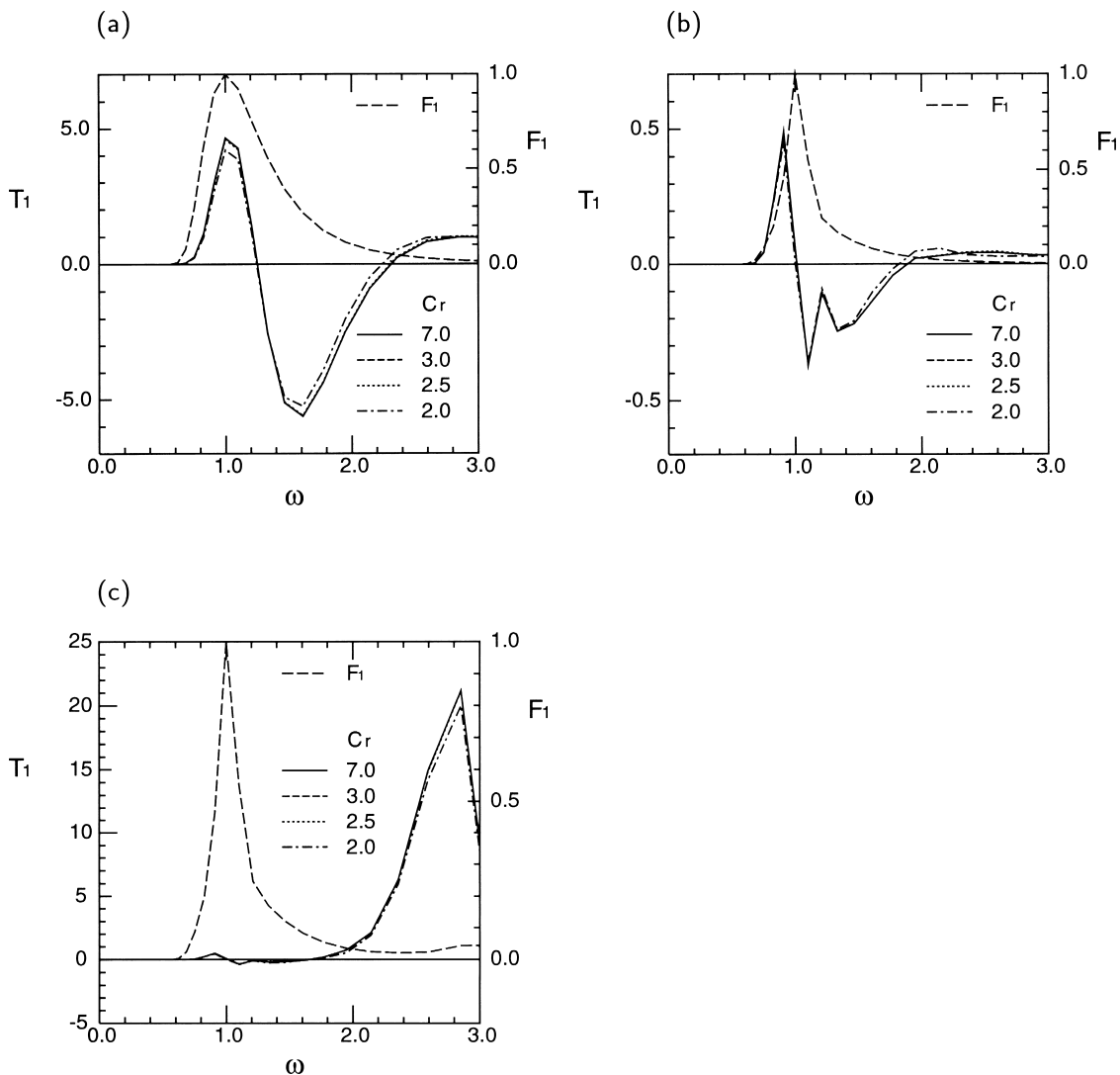


Fig. 6. Nonlinear transfer functions T_1 when $C_r = 2, 2.5, 3,$ and 7 for (a) the PM spectrum, (b) the JONSWAP spectrum, and (c) a double-peaked spectrum defined in the text, with $\cos^2\theta$ directional distribution.

The WAM method gives T_1 about twice as large as the RIAM method for the former spectrum of a narrow directional band width, though both methods produce similar patterns of T_1 . For the double-peaked spectrum, the nonlinear energy transfer function T_1 depends crucially on the method used. The RIAM method predicts an almost the same estimate as the Masuda method, whereas the WAM method gives T_1 which is completely different from the exact result both in magnitude and in pattern. This deficiency of the WAM method can be serious, since such a bimodal spectrum occurs in adjustment processes to changing winds; the largest merit of wave models of the third generation has been said to be their adaptability to changing wind fields.

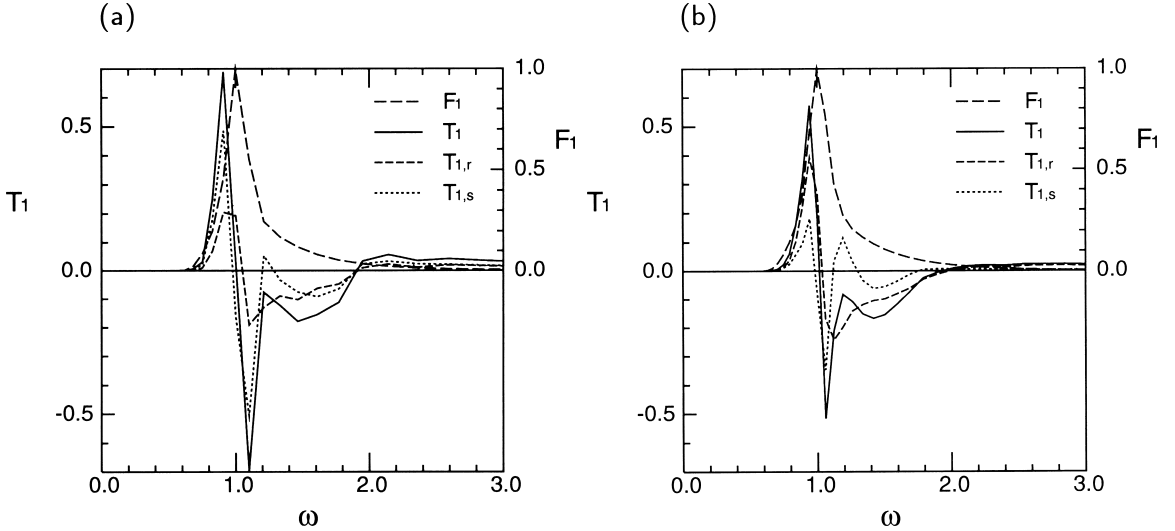


Fig. 7. The one-dimensional nonlinear energy transfer for different grid resolution: (a) $\Delta\theta = 15^\circ$ and $R_\omega = 1.1$, (b) $\Delta\theta = 7.5^\circ$ and $R_\omega = 1.06$, where contributions from singular configuration ($T_{1,s}$), contributions from regular configurations ($T_{1,r}$), and the total transfer function ($T_1 = T_{1,s} + T_{1,r}$) are separately calculated for the same JONSWAP spectrum as in Fig. 2.

2.4 Sensitivity of the RIAM method to parameter values

At the end of this section, we should examine how the performance of the RIAM method depends on various parameter values in typical situations.

2.4.1 Resolution in the frequency and direction: R_ω and $\Delta\theta$

In Fig. 5 we examine the sensitivity of $T_1(\omega)$ to the resolution in the spectral domain for the same JONSWAP spectrum as in Fig. 2. In the former figure $\Delta\theta$ is varied as 30° , 15° , 10° , and 7.5° , while R_ω is fixed at 1.1. On the other hand, the latter figure shows T_1 when R_ω is decreased from 1.12 to 1.06 with fixed $\Delta\theta = 10^\circ$. We observe that the RIAM method nearly converges when $R_\omega = 1.1$ and $\Delta\theta = 10^\circ$, in approximate accordance with the results of Masuda (1980). Therefore, this level of resolution is necessary for practical calculation without significant loss of accuracy.

2.4.2 Truncation of interaction with distant wavenumbers: C_r

Strictly speaking, we have not dealt with all the possible resonance configurations. Even Masuda's algorithm discards the resonance configurations for which the highest frequency ω^{HO} is 7 times as large as the lowest frequency ω^{LO} i.e. $C_r = 7$. From the economical viewpoint the smaller C_r is the more desirable, because it leads to a reduced number of resonance configurations to be processed. The smaller C_r , however, should degrade the accuracy. It is necessary therefore to check the error due to this truncation or cutoff at the ratio C_r on $T(\omega, \theta)$. The question here is to what degree C_r can be lowered without substantial loss of accuracy. Figure 6 indicates the nonlinear energy transfer functions $T_1(\omega)$ when $C_r = 7, 3, 2.5$, and 2, for the PM spectrum, the JONSWAP spectrum, and a double-peaked spectrum $F_1(\omega) = F_J(\omega; 3.3) + 0.05 \times F_J(\omega/3; 3.3)$, where the $\cos^2\theta$ directional distribution is assumed irrespective of the frequency spectrum. Since T appears to be settled when $C_r \geq 3$ even for the double-peaked spectrum, we conclude that $C_r = 3$ is sufficient for practical use. By reducing C_r from 7 (the Masuda method) to 3 (the RIAM

method), we can save computational time by a factor of 3. It is to be noted that the ratio $C_r = \max\{\omega^{HO}/\omega^{LO}\} = 3$ corresponds to $\max\{|\mathbf{k}^{HO}|/|\mathbf{k}^{LO}|\} = 9$ with respect to the wavenumber.

2.4.3 Contributions from singular resonance configurations

As was shown in Masuda (1980), all the resonance configurations are classified into singular and regular configurations (points) in the Boltzmann integral in the RIAM method, which owes its accuracy and stability to the semi-analytical calculation of singular configurations. We quantify how important the contribution from singular configurations is in the total nonlinear energy transfer $T_1(\omega)$. For the same JONSWAP spectrum as in Fig. 2, Fig. 7 compares T_1 obtained with and without the contributions from singular configurations for two kinds of resolution: (a) $\Delta\theta = 15^\circ$, $R_\omega = 1.1$ and (b) $\Delta\theta = 7.5^\circ$, $R_\omega = 1.06$. The regular configurations shares the major portion of the total energy transfer function in the finer resolution, as is expected. The contribution from singular configurations, however, cannot be neglected for a practically reasonable level of resolution $\Delta\theta \geq 10^\circ$. It is preferred therefore to process singular configurations since it improves the accuracy without requiring almost no additional time for computation. It is to be added that, though lowering the accuracy, careful exclusion of singular configurations makes it possible to avoid the numerical instability or spurious ruggedness that is observed almost always in the EXACT-NL method (Hasselmann and Hasselmann, 1985; Young *et al.*, 1987).

We thus conclude the section by recommending parameter values $R_\omega = 1.1$, $\Delta\theta = 10^\circ$, and $C_r = 3$, as a result of the trade-off between economy and accuracy. Singular configurations are to be processed for these parameter values. All the numerical experiments described in the next section were carried out with these values of parameters.

3. Duration-Limited Evolution of Wave Spectra: the RIAM Method in Comparison with the WAM Method

A wave model with the RIAM method incorporated is applied to the duration-limited evolution of wind-wave spectra for various conditions of winds and initial spectra. The results are compared with those obtained with a model with the WAM method incorporated to elucidate the difference due to the different algorithms for nonlinear energy transfer.

Details of the wave model such as the integration scheme will be presented in another paper in preparation, so that we here describes only the parameterization of the other source terms. Our approach here is almost similar to that of the WAM model as follows (WAMDI Group, 1988). The energy input I due to wind follows the formula by Snyder *et al.* (1981)

$$I(\omega, \theta) = \max\left\{0, 0.25 \frac{\rho_a}{\rho_w} \left(28 \frac{u_*}{C_p} \cos(\theta - \theta_w) - 1\right)\right\} \omega F(\omega, \theta) \geq 0, \quad (23)$$

where ρ_a and ρ_w are the densities of air and water, respectively, C_p is the phase velocity of the component wave, and u_* denotes the friction velocity, which is related with the wind speed U_{10} at 10 m height through the drag coefficient C_D due to Wu (1982)

$$C_D = (0.8 + 0.065U_{10}) \times 10^{-3}. \quad (24)$$

The energy dissipation D is parameterized by the formula proposed by Komen *et al.* (1984)

$$D(\omega, \theta) = -2.33 \times 10^{-5} \hat{\omega} \left(\frac{\omega}{\hat{\omega}} \right)^2 \left(\frac{\hat{\alpha}}{\hat{\alpha}_{\text{PM}}} \right)^2 F(\omega, \theta), \quad (25)$$

where $\hat{\omega}$ is the characteristic frequency of the spectrum defined by

$$\hat{\omega} \equiv \frac{E}{\int_0^\infty \omega^{-1} F_1(\omega) d\omega} \quad (26)$$

with

$$E \equiv \int_0^\infty F_1(\omega) d\omega, \quad (27)$$

and $\hat{\alpha}$ is the nonlinearity

$$\hat{\alpha} = \frac{E \hat{\omega}^4}{g^2}, \quad (28)$$

which becomes $\hat{\alpha}_{\text{PM}} = 3.014 \times 10^{-3}$ for the PM spectrum. The high-frequency tail above the cut-off frequency ω_{hf} is dealt with just as in the WAM model (WAMDI Group, 1988): $F_1(\omega) = F_1(\omega_{\text{hf}})(\omega/\omega_{\text{hf}})^{-4}$ and $S(\omega, \theta) = S(\omega_{\text{hf}}, \theta)$ for $\omega \geq \omega_{\text{hf}}$. In this section, the experimental results are presented chiefly in nondimensional units based on the friction velocity u_* and the gravitational

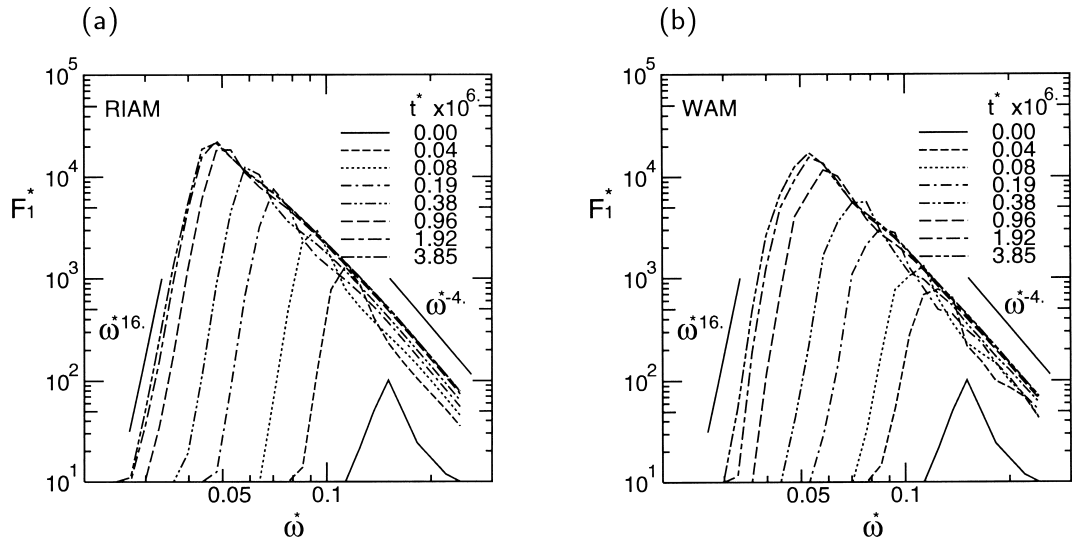


Fig. 8. Duration-limited evolution of the nondimensional frequency spectrum $F_1^* = F_1 g^3 / u_*^5$, obtained by (a) the RIAM method and (b) the WAM method, where $\omega^* = \omega g / u_*$ is the nondimensional frequency. The solid line shows the initial spectrum of the standard JONSWAP form.

acceleration g . The frequency normalized by the spectral peak frequency and the one-dimensional spectrum normalized by its peak value are denoted by $\tilde{\omega}$ and \tilde{F}_1 , respectively.

3.1 Growth by the steady wind

We first examine the temporal evolution of wave spectra under the steadily blowing wind. As the initial spectrum we set the standard JONSWAP frequency spectrum together with $\cos^2\theta$ directional distribution, where the peak frequency ω_p and Phillips' α correspond to those of the PM spectrum for $U_{10} = 5$ m/s. At the moment of $t = 0$ we let the wind speed increase to $U_{10} = 20$ m/s with the wind direction as ever.

Figure 8 shows the evolution of the frequency spectrum, where time integration was carried out with $\Delta t = 10$ min ($\Delta t^* = 6.42 \times 10^3$) till $t = 100$ hours ($t^* = 3.85 \times 10^6$), when the spectrum seemed to have achieved an almost saturated state. The spectrum grows in different manners with different methods for calculating nonlinear energy transfer functions. The RIAM method predicts faster growth of the spectral density than the WAM method. Also the spectral forms differ from each other. It is to be noted, however, that self-similar growth of spectra is realized in both methods (Fig. 8).

Figure 9 shows the evolution of spectral density at several frequencies, where the frequency spectrum $F_1(\omega)$ is normalized by its saturated value $F_{1,\infty}(\omega)$, or more correctly, $F_1(\omega)$ at $t = 100$ hours ($t^* = 3.85 \times 10^6$). We find that both the RIAM and WAM methods reproduce not only the overshoot but also undershoot around the saturated spectral density (Barnett and Sutherland, 1968, Mitsuyasu, 1969), though the undershoot is less conspicuous in the latter method. This result is in contrast with the conclusion of Young *et al.* (1987), who reported that the WAM method failed in reproducing the undershoot by comparing the EXACT-NL model with the WAM model. This discrepancy about the reproducibility of undershoot by the WAM method

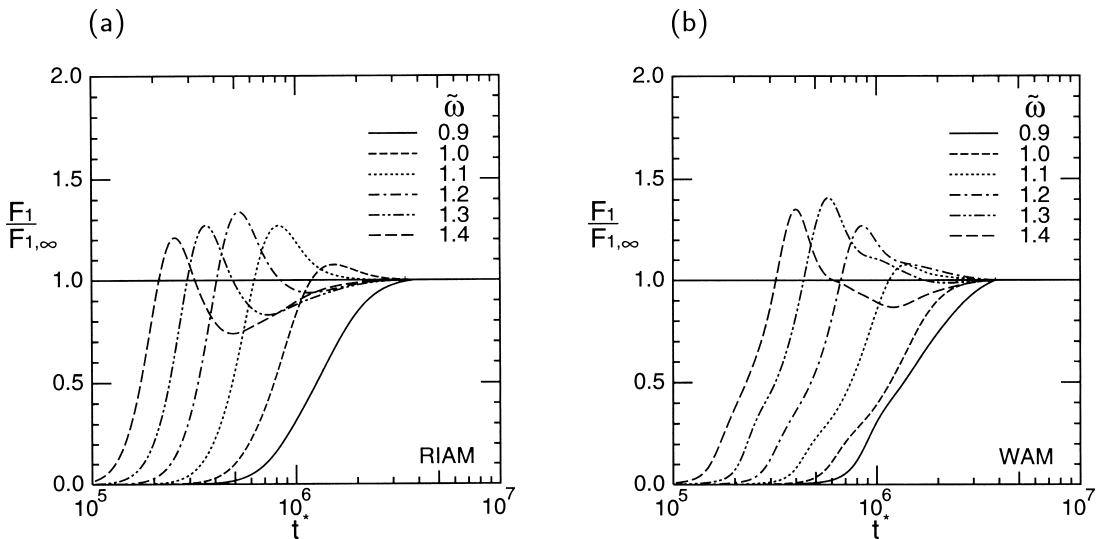


Fig. 9. The time evolution of particular frequency components $F_1(\omega)/F_{1,\infty}(\omega)$ obtained by (a) the RIAM method and (b) the WAM method, where $F_{1,\infty}$ is the saturated value of F_1 and $\tilde{\omega}$ denotes the frequency normalized by the peak frequency of the saturated spectrum.

might be ascribed to difference in schemes for time integration.

As representative macroscopic quantities of wind-wave spectra, Fig. 10 shows the growth of the nondimensional significant wave height H^* and dominant period P^* which are defined by

$$H^* = \frac{4g}{u_*^2} \times \sqrt{E} \quad \text{and} \quad P^* = \frac{2.2\pi u_*}{g} \times \frac{\int_{\Omega_p} \omega^{-1} F_1(\omega) d\omega}{\int_{\Omega_p} F_1(\omega) d\omega}, \quad (29)$$

respectively, in terms of frequency spectra, where the latter integration is made over Ω_p , five frequency bins around the spectral peak frequency. That integration is a simplest kind of filter for more appropriate selection of the peak frequency than the nominal central frequency of the bin that has the maximum spectral density. We see that both H^* and P^* grow faster and approach higher values by the RIAM method than by the WAM method. Note that their asymptotic values obtained here are a little smaller than familiar ones. For example, the present WAM method gives $H_{\infty}^* = 90.1$ and $P_{\infty}^* = 130$ which is to be compared with $H_{\infty}^* \geq 120$ and $P_{\infty}^* \geq 122$ predicted by the WAM model used by Tolman (1992). Also the final values obtained with the RIAM method are $H_{\infty}^* = 101$ and $P_{\infty}^* = 142$, which are less than $H_{\infty}^* = 132$ and $P_{\infty}^* = 188$ expected from Wilson's formula (Wilson, 1965). It appears that the discrepancy does not imply the worse performance of the present method, but suggests some deficiency in the wave model itself used here. The detailed argument, however, will be provided in the next paper in preparation.

Another interesting aspect is found in the evolution of the so-called *Toba's constant* $B \equiv H^* P^{*-3/2}$. At the initial moment it takes 0.029, which is rather lower than its standard value $B_T = 0.062$ (Toba, 1972). It soon increases to a value close to the standard value B_T , adjusting to the new wind condition. We note that both the RIAM method and the WAM method yield almost the same asymptotic values of $B = H^* P^{*-3/2}$, though the two methods give rather different

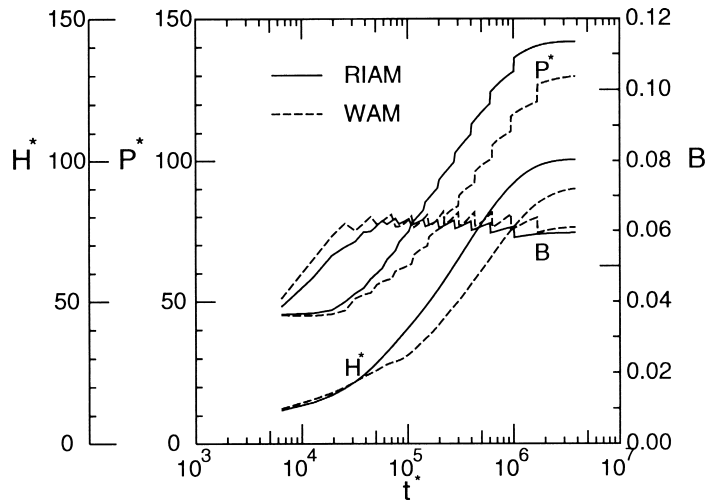


Fig. 10. The evolution of the nondimensional significant wave height H^* , dominant period P^* , and $B \equiv H^* P^{*-3/2}$, where $t^* = tu_*/g$ is the nondimensional duration time. The results of the RIAM method is denoted by solid lines and those of the WAM method by dashed lines.

saturated values for H^* and P^* themselves. Judging from the way B approaches the saturation value, we observe that local equilibrium is attained within $t^* \lesssim 4 \times 10^4$ ($t \lesssim 1.04$ hours) for the WAM method, while $t^* \lesssim 8 \times 10^4$ ($t \lesssim 2.08$ hours) for the RIAM method. Another noteworthy phenomenon is that B overshoots, then undershoots, and finally approaches the final value from below to $B_\infty = 0.06 \simeq B_T$ in both methods.

3.2 Saturated spectra

Long time integration over $t = 100$ hours ($t^* = 3.85 \times 10^6$) yielded *nearly* saturated spectra as is observed in the preceding logarithmic plot in Fig. 8. On the low-frequency side, the saturated spectra obtained by the two methods have slightly different slopes. Also we note that the spectrum through the RIAM method has a narrower transition zone from low to high frequencies. Toward higher frequencies, the frequency spectrum decreases as, but slightly more slowly than, ω^{-4} irrespective of the method for nonlinear energy transfer T .

The saturated spectra obtained with the RIAM and WAM methods are distinguished from each other better in the linear normalized plot of Fig. 11, where the spectral peak frequency and the peak density are unity. We observe that the saturated frequency spectra are far from the PM spectrum, which has long been envisaged as the saturated spectrum. On both sides of the peak frequency, either method yields a similar form that is broader than the JONSWAP spectrum but narrower than the PM spectrum. A closer examination shows that the spectrum around the peak frequency obtained with the RIAM method is steeper than that of the WAM method.

Two-dimensional distributions $F^*(\omega_x^*, \omega_y^*) \equiv F^*(\omega^*, \theta)\omega^*$ of saturated spectra are examined in contours (Fig. 12) and angular distribution functions $S(\omega, \theta) = F(\omega, \theta)/F_1(\omega)$ at several frequencies (Fig. 13). In comparison with the RIAM method the WAM method gives a narrow and concentrated directional distribution at high frequencies with almost no energy distributed to $|\theta| \geq 120^\circ$. The most curious aspect at high frequencies is that the directional distribution seems to approach a certain bimodal one in both methods. Similar features were reported, however, by Banner and Young (1994), who dealt with the fetch-limited evolution with the rigorous method of Resio and Perrie (1991). On the low frequency side of the peak frequency ($\tilde{\omega} = 0.8$), a unimodal directional distribution appears for the RIAM method, but a conspicuous bimodal feature is observed for the WAM method. The bimodal distribution obtained with the WAM method is presumably a spurious consequence of the insufficient approximation of the WAM method as was pointed out before in Fig. 3.

Remarkable differences in directional distributions are found not only between the RIAM and WAM models, but also between these model results and the empirical one either by Mitsuyasu *et al.* (1975) and Hasselmann *et al.* (1980) or by Donelan *et al.* (1985) shown in Fig. 13(c) or (d), respectively; see 2.2 for the formulas for those empirical directional distributions. Near the peak frequency, both models predict lower concentration of energy near the main direction than the empirical ones. The directional concentration of the RIAM method, however, is similar to the distribution of Mitsuyasu *et al.* (1975) or Hasselmann *et al.* (1980) rather than that by Donelan *et al.* (1985), which predicts much more concentrated distribution near the peak frequency. In general the empirical ones have notable energy in wide angles, whereas the directional distribution of the models shows a rapid decay away from $\theta - \bar{\theta} \sim \pm 90^\circ$. The most interesting difference at high frequencies is that the models yield directional distributions with two maxima at two oblique angles while empirical formulas assert unimodal distributions with a peak along the wind direction. The former double-peaked structure at high frequencies is presumably a consequence in the present wave models. A serious degree of uncertainty both in

model formulation and in measurement at the sea, however, prevent us from determining which directional distribution describes the real spectra best.

The different methods for calculating T thus yield different saturated spectra $F(\omega, \theta)$, suggesting different energy balance in different models. Here, however, we do not get into details about why the saturated spectrum differs between the two models or between the models and the empirical ones. Such arguments will be addressed in the next paper.

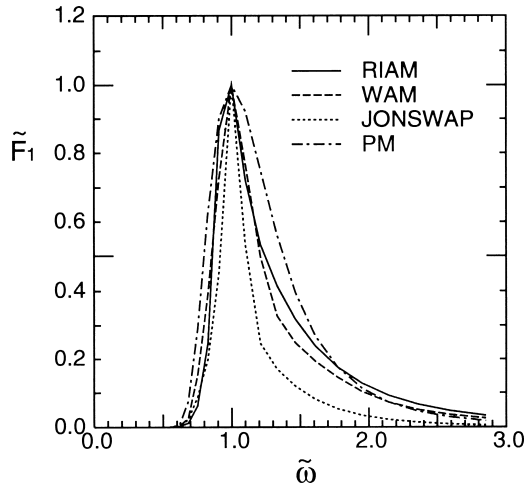


Fig. 11. Normalized forms of saturated frequency spectra \tilde{F}_1 obtained by the RIAM method and the WAM method. The standard JONSWAP spectrum and the PM spectrum are shown for reference.

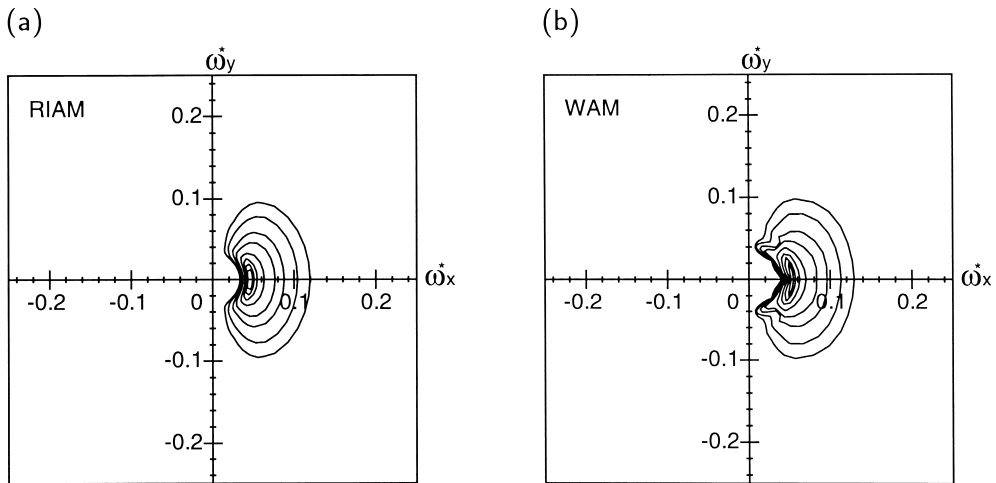


Fig. 12. Contours of the two-dimensional saturated spectrum $F^*(\omega_x^*, \omega_y^*) \equiv F^*(\omega^*, \theta) \omega^*$ obtained by (a) the RIAM method and (b) the WAM method, where the contours are (a) $4.09 \times 10^3, 8.18 \times 10^3, 2.04 \times 10^4, 4.09 \times 10^4, 1.02 \times 10^5, 2.04 \times 10^5, 3.07 \times 10^5,$ and 3.68×10^5 , and (b) $2.63 \times 10^3, 5.26 \times 10^3, 1.31 \times 10^4, 2.63 \times 10^4, 6.57 \times 10^4, 1.31 \times 10^5, 1.97 \times 10^5,$ and 2.37×10^5 , respectively.

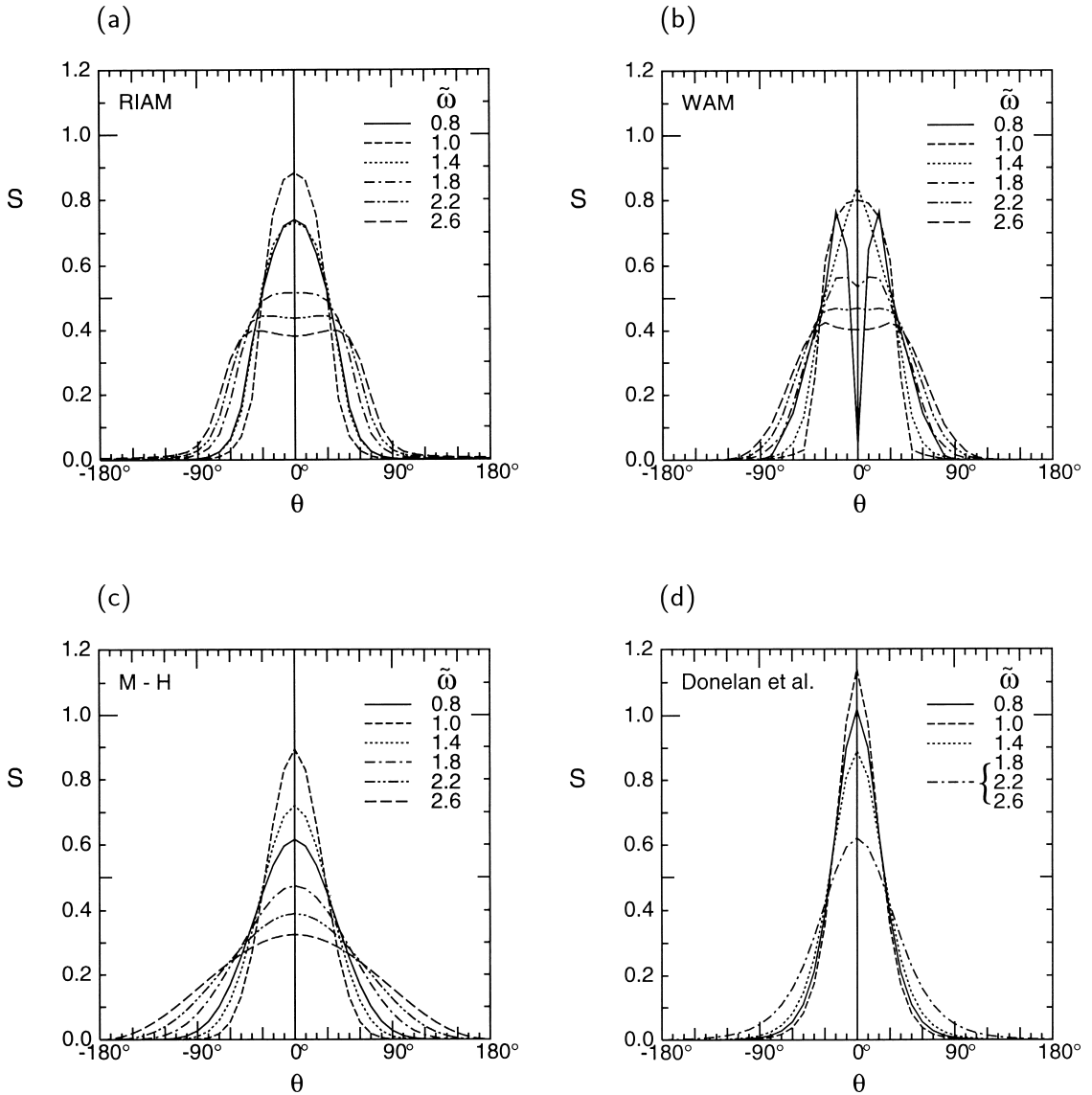


Fig. 13. The directional distributions $S(\omega, \theta) = F(\omega, \theta)/F_1(\omega)$ at several frequencies for the saturated spectra obtained by (a) the RIAM method and (b) the WAM method, together with those of (c) the Mitsuyasu-Hasselmann type, and (d) the Donelan type.

3.3 Adjustment to the abrupt change of the wind direction

The utility of the third-generation model has often been said to lie in its ability to predict the adjustment of wave spectra to sudden changes of wind directions. We therefore examine how differently spectra respond to the change of wind directions when different schemes for T are used. Consider an initial frequency spectrum of the standard JONSWAP type, where the peak frequency and Phillips' α correspond to those of the PM spectrum for $U_{10} = 10$ m/s. We assume a frequency-independent directional distribution of $\cos^2 \theta$ type with $\bar{\theta} = \bar{\theta}_i = 0^\circ$, which is referred

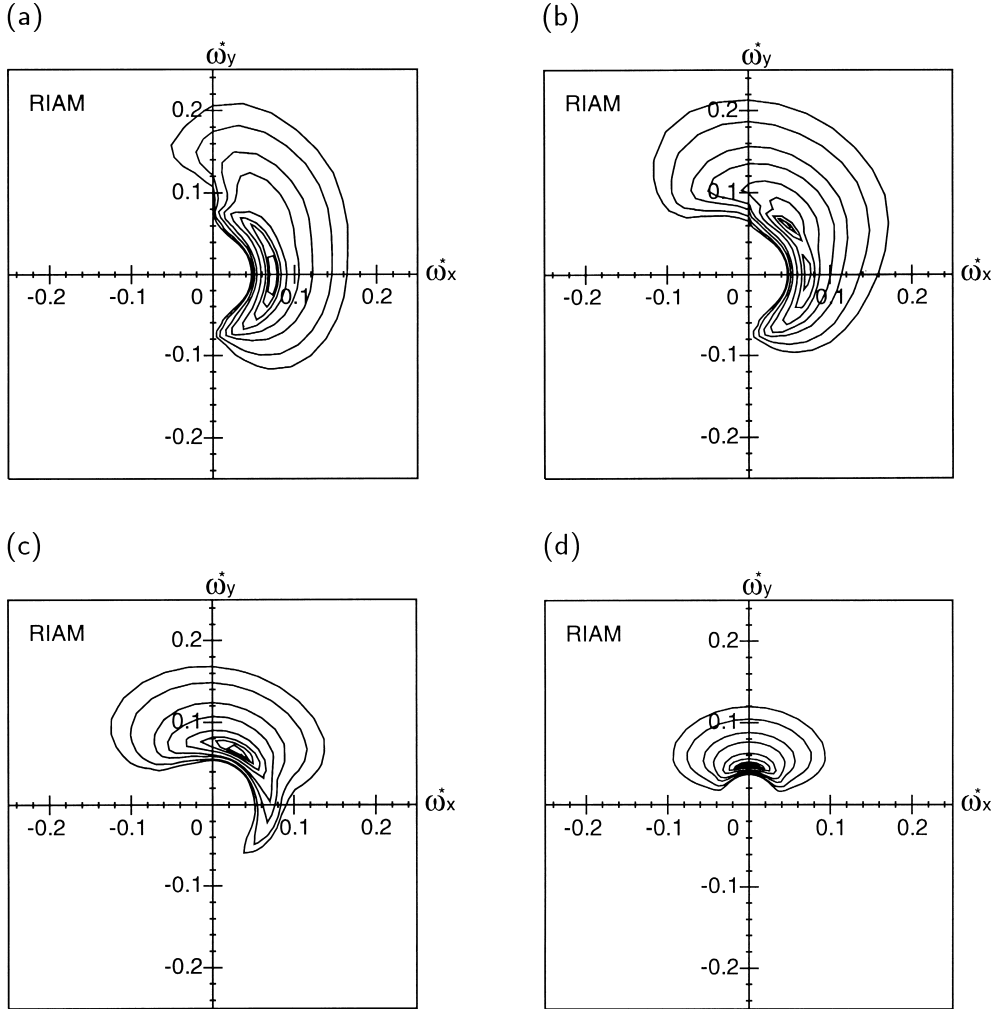


Fig. 14. Evolution of the two-dimensional spectrum $F^*(\omega_x^*, \omega_y^*)$ obtained by the RIAM method for the initial JONSWAP spectrum with $\cos^2\theta$ directional distribution: (a) $t = 1$ hours, (b) $t = 2$ hours, (c) $t = 5$ hours, and (d) $t = 30$ hours. The contours are (a) 1.97×10^2 , 3.95×10^2 , 9.88×10^2 , 1.98×10^3 , 4.94×10^3 , 9.88×10^3 , 1.48×10^4 , and 1.78×10^4 , (b) 2.01×10^2 , 4.03×10^2 , 1.01×10^3 , 2.01×10^3 , 5.04×10^3 , 1.01×10^4 , 1.51×10^4 , and 1.81×10^4 , (c) 6.09×10^2 , 1.22×10^3 , 3.05×10^3 , 6.09×10^3 , 1.52×10^4 , 3.05×10^4 , 4.57×10^4 , and 5.48×10^4 , and (d) 4.00×10^3 , 8.00×10^3 , 2.00×10^4 , 4.00×10^4 , 1.00×10^5 , 2.00×10^5 , 3.00×10^5 , and 3.60×10^5 .

to as the *initial direction* of the wave spectrum. At $t = 0$ we let the wind change abruptly: the wind speed is increased to $U_{10} = 20$ m/s and the wind direction is rotated anticlockwise by a right angle toward the direction of $\bar{\theta}_n = 90^\circ$, which we refer to as the *new direction*. Figures 14 and 15 show different stages of the evolution of the two-dimensional spectrum $F^*(\omega_x^*, \omega_y^*) \equiv F^*(\omega^*, \theta)\omega^*$ for the RIAM method and the WAM method, respectively, at $t = 1, 2, 5,$ and 30 hours ($t^* = 3.85 \times 10^4, 7.70 \times 10^4, 1.92 \times 10^5,$ and 1.15×10^6). The evolution of spectral density in the initial direction $\bar{\theta}_i$ and the new direction $\bar{\theta}_n$ are shown in Figs. 16 and 17 for the RIAM and WAM methods, respectively.

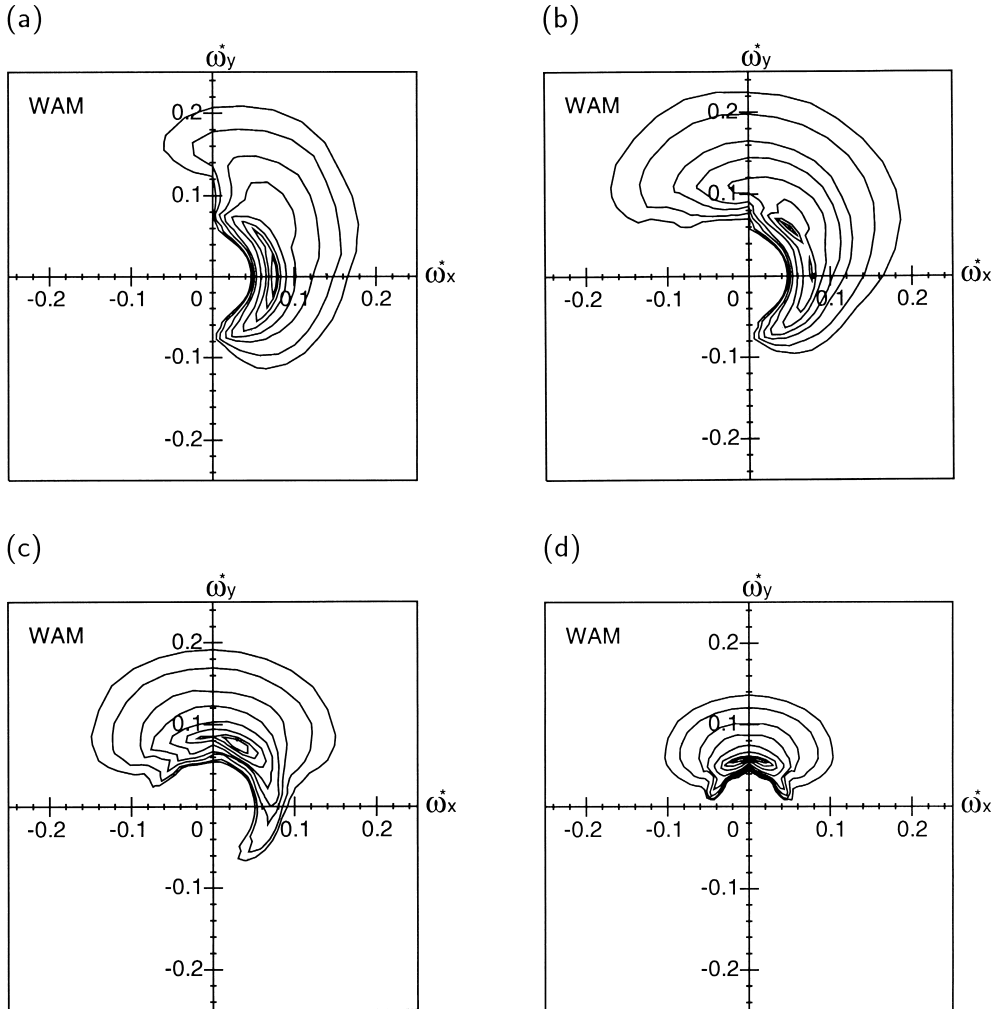


Fig. 15. The same as Fig. 14 except that the results are obtained by the WAM method. The contours are (a) 2.05×10^2 , 4.10×10^2 , 1.03×10^3 , 2.05×10^3 , 5.13×10^3 , 1.03×10^4 , 1.54×10^4 , and 1.85×10^4 , (b) 1.61×10^2 , 3.22×10^2 , 8.04×10^2 , 1.61×10^3 , 4.02×10^3 , 8.04×10^3 , 1.21×10^4 , and 1.45×10^4 , (c) 3.09×10^2 , 6.18×10^2 , 1.54×10^3 , 3.09×10^3 , 7.72×10^3 , 1.54×10^4 , 2.32×10^4 , and 2.78×10^4 , and (d) 1.90×10^3 , 3.80×10^3 , 9.51×10^3 , 1.90×10^4 , 4.75×10^4 , 9.51×10^4 , 1.43×10^5 , and 1.71×10^5 .

We see that the energy of the peak spectral frequency once decreases at the initial stage. This is simply because energy-containing waves propagating in the initial direction suffer enhanced dissipation but no energy is supplied from the wind blowing to the right angle. The decrease in the spectral energy in the initial direction is observed in both methods, but it is larger in the WAM model than in the RIAM model. The spectral density begins to increase at higher frequencies adjusting to the new wind condition. The secondary peak thus appears at a high frequency in a direction that is close to the new direction but slightly deviated toward the initial direction. A noteworthy phenomenon is that the spectral density at the initial direction shows a clear

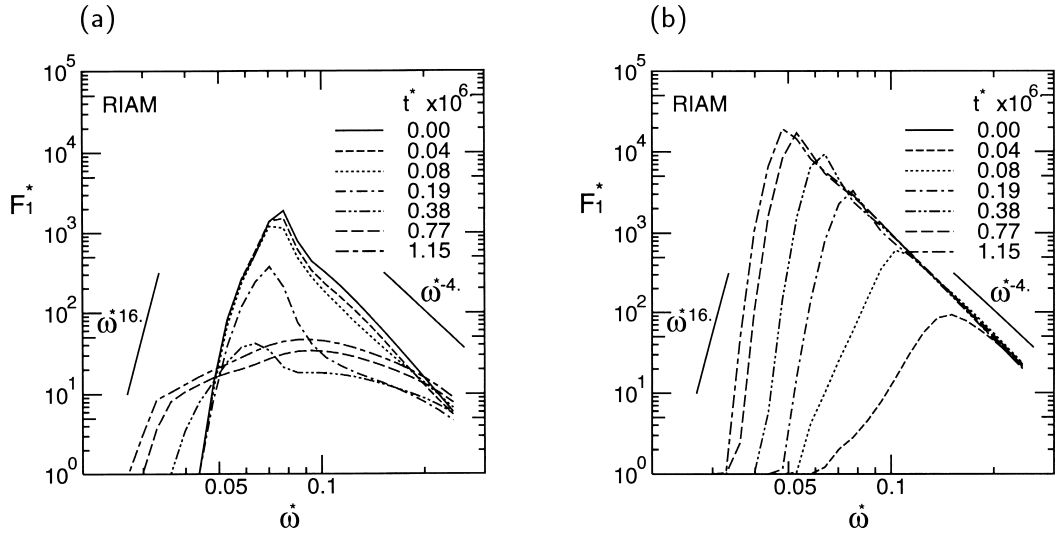


Fig. 16. Evolution of the spectral density $F^*(\omega^*, \theta)$ obtained with the RIAM method for (a) the direction of $\theta = \theta_i = 0^\circ$ and (b) the direction of $\theta = \theta_n = 90^\circ$.

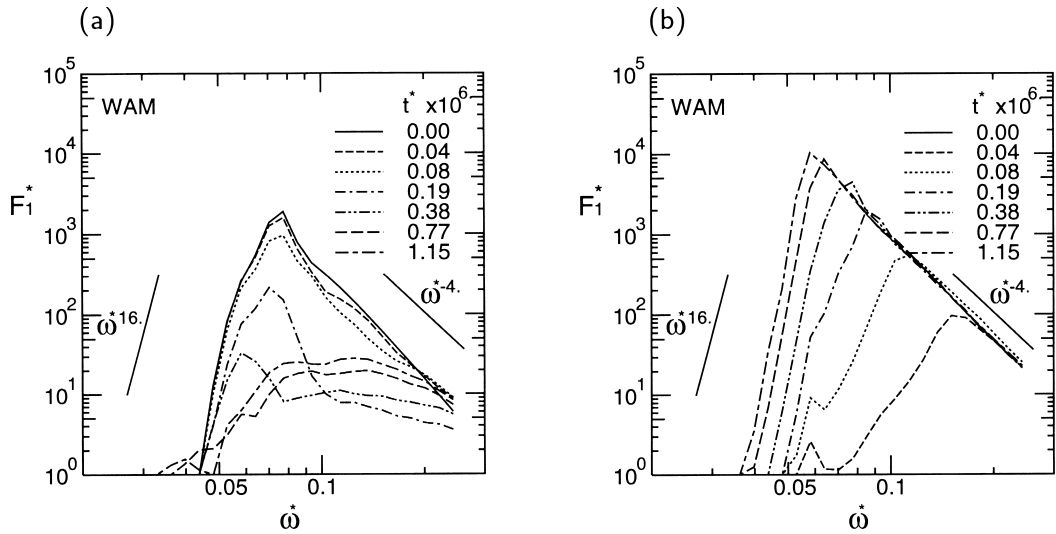


Fig. 17. The same as Fig. 16 except through the WAM method.

frequency downshift in the RIAM model, whereas no such tendency is observed in the WAM model. The spectral density in the new direction grows in a way similar to that of F_1 under the steady wind (Fig. 8). In the case of the WAM method, however, a curious hump near $\omega^* \approx 0.06$ was observed for a while. After $t = 30$ hours ($t^* = 1.15 \times 10^6$), in both methods, frequency spectra and directional distributions become almost the same as at the saturated state discussed in Subsection 3.2, except for the scale, magnitude, and main direction.

3.4 Response to the perturbation to the locally equilibrated spectral form

Nonlinear energy transfer has often been referred to as the most important agent that stabilizes the spectral form as it is observed actually. Masuda (1980) tested this problem by adding a small spectrum to a standard form of spectrum. Although he did not carry out time integration, he showed that T at the initial moment works to smooth out the spectral ruggedness.

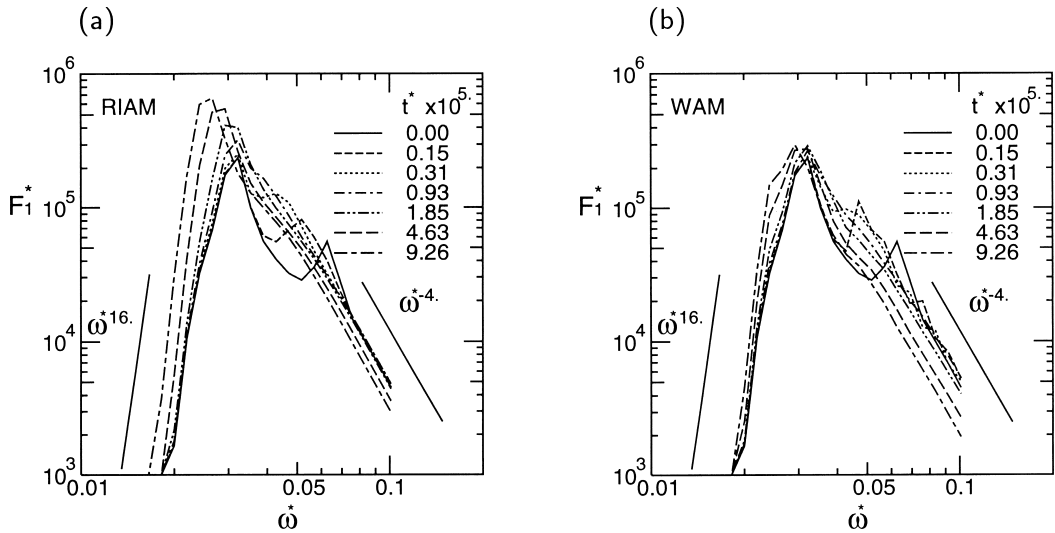


Fig. 18. Evolution of the one-dimensional frequency spectrum $F_1^*(\omega^*)$ for the initial spectrum perturbed by a small hump $F_1(\omega) = F_J(\omega; 3.3) + 0.2 \times F_J(\omega/2; 3.3)$, where the angular distribution function is $\cos^2\theta$ irrespective of the frequency and input I and dissipation D are discarded.

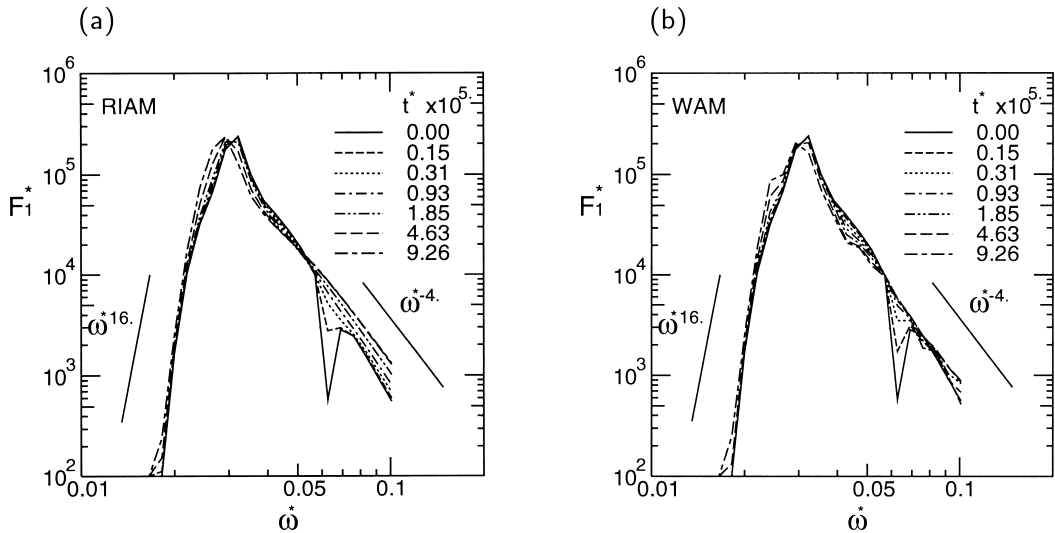


Fig. 19. The same as in Fig. 18 except that the initial frequency spectrum is perturbed by a small depression $F_1(\omega) = F_J(\omega; 3.3) - 0.03 \times F_J(\omega/2; 9)$.

This problem was later investigated by Resio and Perrie (1991) for a bump or by Young and Van Vledder (1993) for a depression. Using rigorous algorithms, they carried out time integration to confirm that the perturbed spectrum recovers its original smooth form. Masson (1993) also discussed the problem of a hump in relation to the nonlinear coupling between swell and wind waves.

The similar problems are investigated here in order to compare the performance of the RIAM method with that of the WAM method for three kinds of initial spectra: (1) spectrum perturbed by a small hump

$$F(\omega, \theta) = (F_J(\omega; 3.3) + 0.2 \times F_J(\omega / 2; 3.3)) \hat{S}(2) \cos^2 \theta, \tag{30}$$

(2) spectrum perturbed by a small depression

$$F(\omega, \theta) = (F_J(\omega; 3.3) - 0.03 F_J(\omega / 2; 9)) \hat{S}(2) \cos^2 \theta, \tag{31}$$

and (3) spectrum with a very narrow frequency band ($\gamma = 9$)

$$F(\omega, \theta) = F_J(\omega; 9.0) \hat{S}(2) \cos^2 \theta, \tag{32}$$

where the peak frequency ω_p and Phillips' α correspond to those of the PM spectrum for $U_{10} = 10$ m/s. In this subsection, we discard I and D as in Resio and Perrie (1991), so that the spectral evolution is governed by nonlinear energy transfer T only.

Figures 18 to 20 show the evolution of F_1 for the three initial spectra above, respectively, predicted with the RIAM method and the WAM method. We see that nonlinear energy transfer removes the hump or the depression to recover the original smooth spectral form, as was pointed

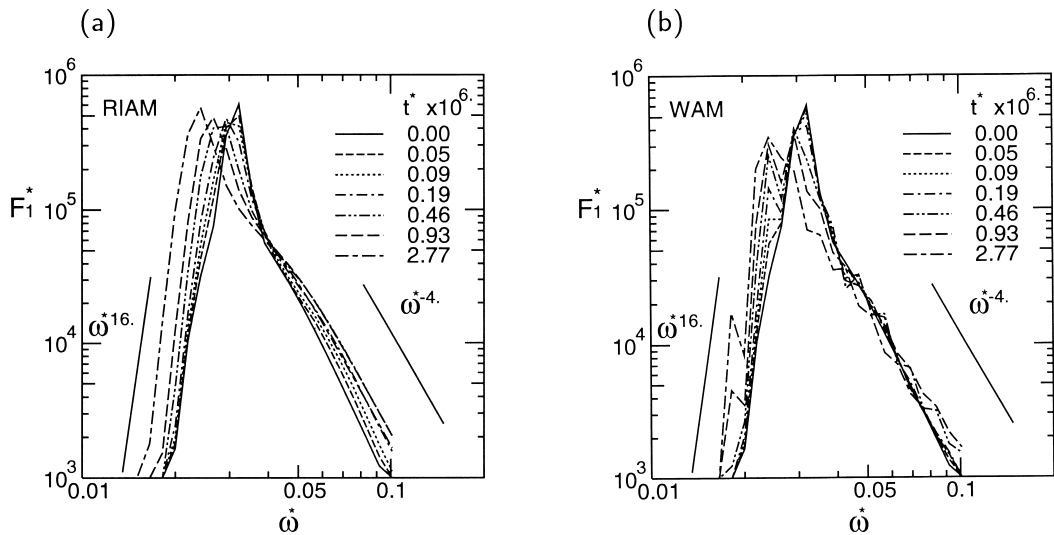


Fig. 20. The same as in Fig. 18 except that the initial spectrum has a narrow band width ($\gamma = 9$) $F_1(\omega) = F_J(\omega; 9)$.

out by Masuda (1980), Resio and Perrie (1991), and Young and Van Vledder (1993). Also the too narrow spectrum is changed into a broader moderate one. In these figures, we see that the RIAM method represents the restoring roles of nonlinear energy transfer in a smooth regular way. On the other hand the WAM method yields other unrealistic bumps or depressions during the adjusting process.

4. Summary and Discussions

A new scheme called the RIAM method was developed to calculate efficiently the nonlinear energy transfer function among wind waves. In this scheme, the symmetric properties of wave resonance are fully incorporated into the rigorous method of Masuda (1980). Thus, the RIAM method inherits the accuracy from Masuda's algorithm (1980) and the computational efficiency from the discrete interaction approximation of Hasselmann *et al.* (1985).

The accuracy and computational efficiency of the RIAM method were examined in comparison with other previous methods by applying them to some typical spectra. The RIAM method turned out to have the same degree of accuracy as the other previous rigorous methods. As processing singular points adequately, the RIAM method proved much better than the Hasselmann and Hasselmann method (1981) in numerical stability or smoothness. In addition the RIAM method is 300 times faster than the original Masuda method. As regards to the Resio and Perrie method, it required 20 min = 1200 sec on an IBM-PC with an accelerator board to calculate the nonlinear energy transfer for a given spectrum (Resio and Perrie, 1991), while the RIAM method consumes 1 sec on an HP-735 Work Station for the same job. Unfortunately, however, it is difficult to compare the efficiency of the two methods because of different machines, different resolution, and others. In any case, the RIAM method belongs to the fastest schemes in the (semi-)rigorous algorithms. The RIAM method is thus capable of computing nonlinear energy transfer functions almost to the accuracy of rigorous methods in much less computational time.

Then the performance of the RIAM method was compared with that of the WAM method, a representative one in operational use. The RIAM method still requires about 2000 times more computational time than the WAM method, simply because the former processes about 2000 configurations of resonance while the latter only one. It was shown, however, that the WAM method gives quite unrealistic nonlinear energy transfer functions both in magnitude and in pattern, when the spectrum is either directionally concentrated, frequency-concentrated, or double-peaked; the WAM method is unreliable even for the standard JONSWAP spectrum. In short, the RIAM method has a much wider range of validity and better accuracy than the WAM method.

In addition, the parameter sensitivity of the performance of the RIAM method was investigated to give desirable values of parameters for the method to operate in a practical level of computational time without losing substantial accuracy. The proposed values are $R_\omega = 1.1$, $\Delta\theta = 10^\circ$, and $C_r = 3$. Also it is recommended to process singular points (configurations) since it improves accuracy without almost no additional time for computation.

The performance of the RIAM method was examined as well in the temporal evolution of wave spectra. We assumed the same formulas of source terms as the WAM model except for the nonlinear term. We first investigated the growth of wind waves under the steadily blowing wind. It was shown that the peak period and the total energy of wind waves grow faster by the RIAM method than by the WAM method. Nevertheless, Toba's constant of his 3/2-power law asymptotically approaches the standard value about 0.06 in both methods. The saturated wave

energy and dominant peak frequency were a little smaller than those reported so far with previous WAM models or those predicted by Wilson's formula. Not only the RIAM method but also the WAM method could reproduce well both overshoot and undershoot phenomena, which is in contrast with the conclusion of Young *et al.* (1987), who reported that the WAM model could not realize undershoot.

Even after a long-run, the spectrum does not approach the Pierson-Moskowitz spectrum, but it seems to have achieved an almost saturated one, irrespective of the two methods. On the low-frequency side of the peak frequency, the spectrum obtained by the RIAM method is steeper than the JONSWAP spectrum, in agreement with a finding for the evolution of wind-wave spectra in a wind flume (Kusaba and Masuda, 1988). On the other hand, the WAM method gives the spectrum with a broader band width around the peak frequency. Furthermore, the WAM method yields the angular distribution function with two oblique maxima in front of the peak frequency. This double-peaked directional distribution is not found for the spectrum predicted by the RIAM method. A closer examination suggests that this is due to the insufficient approximation of the WAM method.

We found a curious feature of saturated spectra at high frequencies, commonly to either method. The angular distribution function attains its maximum at the angles of $\pm 40^\circ$ or more from the main propagation direction. Though for the fetch-limited growth, a similar structure was pointed out by Banner and Young (1994), who ascribed this bimodal angular spreading to the unsuitable assumptions about the ambiguous empirical formula for energy dissipation and about the spectral tail in the frequency domain. On the other hand, the frequency spectrum decreases approximately as but slightly slower than ω^{-4} at high frequencies in both the RIAM and the WAM methods.

Then we examined the response of wave spectra to the abrupt turning of the wind direction by a right angle. We see that the spectral energy decreases more in the WAM method than in the RIAM method. At the later stage, both methods yield the secondary peak located at high frequencies with its direction close to the new direction of the wind but slightly shifted to the initial direction. In the initial main direction, the spectrum shows an evident transfer of energy toward lower frequencies, while such a downshift is not produced by the WAM method.

To examine the stabilizing role of nonlinear energy transfer, we tested the spectral evolution for three forms of initial spectra that are deviated from the moderate and smooth one in the approximate local equilibrium: a spectrum with a small local hump, a spectrum with a small local depression, and a spectrum with an extremely narrow band width. In these experiments, only T was taken into account with the other terms of I and D discarded. The RIAM method effectively smooths out the hump or depression of the spectrum or change the too steep spectrum into that with a moderate band width. Reflecting the basic role of nonlinear energy transfer, the WAM method shows the same tendency of spectral evolution, but produces spurious humps or depressions at other frequencies during the adjusting process.

In this paper, we have restricted ourselves to the description of the computational aspects of the RIAM method such as its algorithm and performance mainly in comparison with the WAM method. The next paper will be devoted to the physics and dynamics of the wave evolution that is realized when the RIAM method is applied together with the other source terms. We will discuss there why bimodal angular spreading occurs in high frequencies, how energy balance is maintained in saturated spectra, or how wave models are to be improved in view of the RIAM method.

Finally, a few remarks should be made about the speed of the RIAM method. As was

mentioned before, the RIAM method deals with a few thousands of configurations of resonant four-waves, in contrast with only one configuration in the WAM method. The RIAM method therefore must necessarily require a few thousands times larger computational time than the WAM method, so that even the efficiency of the RIAM method is far from what is available to operation models for wave forecast today. The advantage of the RIAM method is to give almost the same degree of accuracy as the other exact algorithm such as the Masuda method even for rather *atypical* wave spectra. Therefore, the RIAM method can still be used as an efficient means for theoretical investigation, which is indispensable in order to improve wave models above the empirical level.

In any case, the RIAM method cannot be used as an algorithm for operational wave prediction for the present power of computers. We need to develop a scheme of practical efficiency with a slightly lower level of accuracy for the algorithm to be in daily use. The method required is called a simplified RIAM method (SRIAM method), which processes a diminished number of resonance configurations. Another paper will be directed to the operational model for wave forecasting that incorporates the SRIAM method for calculating nonlinear energy transfer functions.

Acknowledgements

We thank Prof. Mitsuyasu and Prof. Kusaba for their pleasant discussion throughout the work. We also would like to appreciate technical assistance extended by Dr. Uehara and Mr. Ishibashi.

References

- Banner, M. L. and I. R. Young (1994): Modeling spectral dissipation in the evolution of wind waves. Part I: Assessment of existing model performance. *J. Phys. Oceanogr.*, **24**, 1550–1571.
- Barnett, T. P. and A. J. Sutherland (1968): A note on an overshoot effect in wind-generated waves. *J. Geophys. Res.*, **73**, 6879–6885.
- Donelan, M. A., J. Hamilton and W. H. Hui (1985): Directional spectra of wind-generated waves. *Phil. Trans. Roy. Soc. London*, **A315**, 509–562.
- Dungey, J. C. and W. H. Hui (1979): Nonlinear energy transfer in a narrow gravity-wave spectrum. *Proc. Roy. Soc. London*, **A368**, 239–265.
- Fox, M. J. (1976): On the nonlinear transfer of energy in the peak of a gravity-wave spectrum II. *Proc. Roy. Soc. London*, **A348**, 467–483.
- Hasselmann, D. E., M. Dunkel and J. A. Ewing (1980): Directional wave spectra observed during JONSWAP 1973. *J. Phys. Oceanogr.*, **10**, 1264–1280.
- Hasselmann, K. (1962): On the non-linear energy transfer in a gravity-wave spectrum. Part 1. General theory. *J. Fluid Mech.*, **12**, 481–500.
- Hasselmann, K. (1963): On the non-linear energy transfer in a gravity-wave spectrum. Part 2. Conservation theorems; wave-particle analogy; irreversibility. *J. Fluid Mech.*, **15**, 273–281.
- Hasselmann, K., T. P. Barnett, H. Bouws, H. Carlson, D. E. Cartright, K. Enke, J. A. Ewing, H. Gineapp, D. E. Hasselmann, P. Kruseman, A. Meerburg, P. Muller, D. J. Olbers, K. Richter, W. Sell and H. Walden (1973): Measurements of wind wave growth and swell decay during the Joint North Sea Wave Project (JONSWAP). *Dtsch. Hydrogr. Z., Suppl.*, **A8**, No. 12, 95 pp.
- Hasselmann, S. and K. Hasselmann (1981): A symmetrical method of computing the nonlinear transfer in a gravity wave spectrum. *Hamb. Geophys. Einzelschriften, Reihe A: Wiss. Abhand.*, **52**, 138 pp.
- Hasselmann, S. and K. Hasselmann (1985): Computations and parameterizations of the nonlinear energy transfer in a gravity-wave spectrum. Part I: A new method for efficient computations of the exact nonlinear transfer integral. *J. Phys. Oceanogr.*, **15**, 1369–1377.
- Hasselmann, S., K. Hasselmann, J. H. Allender and T. P. Barnett (1985): Computations and parameterizations of the nonlinear energy transfer in a gravity-wave spectrum. Part II: Parameterizations of the nonlinear energy transfer for application in wave models. *J. Phys. Oceanogr.*, **15**, 1378–1391.

- Komatsu, K., T. Kusaba and A. Masuda (1993): An efficient method for computing nonlinear energy transfer among wind waves. *Bull. Res. Inst. Appl. Mech. Kyushu Univ.*, **75**, 121–146 (in Japanese).
- Komen, G. J., S. Hasselmann and K. Hasselmann (1984): On the existence of a fully developed wind-sea spectrum. *J. Phys. Oceanogr.*, **14**, 1271–1285.
- Kusaba, T. and A. Masuda (1988): Wind-wave spectra based on the hypothesis of local equilibrium. *J. Oceanogr. Soc. Japan*, **45**, 45–64.
- Longuet-Higgins, M. S. (1962): Resonant interactions between two trains of gravity waves. *J. Fluid Mech.*, **12**, 321–332.
- Longuet-Higgins, M. S. (1976): On the nonlinear transfer of energy in the peak of a gravity-wave spectrum: A simplified model. *Proc. Roy. Soc. London*, **A347**, 311–328.
- Masson, D. (1993): On the nonlinear coupling between swell and wind waves. *J. Phys. Oceanogr.*, **23**, 1249–1258.
- Masuda, A. (1980): Nonlinear energy transfer between wind waves. *J. Phys. Oceanogr.*, **10**, 2082–2092.
- Masuda, A. (1986): Nonlinear energy transfer between random gravity waves. p. 41–57. In *Wave Dynamics and Radio Probing of the Ocean Surface*, ed. by O. M. Phillips and K. Hasselmann, Plenum Press, New York.
- Mitsuyasu, H. (1969): On the growth of the spectrum of wind-generated waves (II). *Rep. Res. Inst. Appl. Mech. Kyushu Univ.*, **17**, 235–243.
- Mitsuyasu, H., F. Tasai, T. Suhara, S. Mizuno, M. Ohkusu, T. Honda and K. Rikiishi (1975): Observations of the directional spectra of ocean waves using a cloverleaf bouy. *J. Phys. Oceanogr.*, **5**, 750–760.
- Phillips, O. M. (1977): *The Dynamics of the Upper Ocean*. Cambridge Univ. Press, Cambridge, 336 pp.
- Resio, D. and W. Perrie (1991): A numerical study of nonlinear energy fluxes due to wave-wave interactions. *J. Fluid Mech.*, **223**, 603–629.
- Sell, W. and K. Hasselmann (1972): Computations of nonlinear energy transfer for JONSWAP and empirical wind-wave spectra. *Rep. Inst. Geophys. Univ. Hamburg*, 1–6.
- Snyder, R. L., F. W. Dobson, J. A. Elliot and R. B. Long (1981): Array measurements of atmospheric pressure fluctuations above surface gravity waves. *J. Fluid Mech.*, **102**, 1–59.
- The SWAMP Group (24 Authors) (1985): *Ocean Wave Modeling*. Plenum Press, New York, 256 pp.
- The WAMDI Group (13 authors) (1988): The WAM model—A third generation ocean wave prediction model. *J. Phys. Oceanogr.*, **18**, 1378–1391.
- Toba, Y. (1972): Local balance in the air-sea boundary processes. I. On the growth process of wind waves. *J. Oceanogr. Soc. Japan*, **28**, 109–120.
- Tolman, H. L. (1992): Effects of numerics on the physics in a third-generation wind-wave model. *J. Phys. Oceanogr.*, **22**, 1095–1111.
- Webb, D. J. (1978): Non-linear transfers between sea waves. *Deep-Sea Res.*, **25**, 279–298.
- Wilson, B. W. (1965): Numerical prediction of ocean waves in the North Atlantic for December 1959. *Deut. Hydrogr. Zeit.*, Jahrgang **18**, Heft 3, 114–130.
- Wu, J. (1982): Wind-stress coefficients over sea surface from breeze to hurricane. *J. Geophys. Res.*, **87**, 9704–9706.
- Young, I. R. and G. Ph. Van Vledder (1993): A review of the central role of nonlinear interactions in wind-wave evolution. *Phil. Trans. Roy. Soc. London*, **A342**, 505–524.
- Young, I. R., S. Hasselmann and K. Hasselmann (1987): Computations of a wave spectrum to a sudden change in wind direction. *J. Phys. Oceanogr.*, **17**, 1317–1338.